AD-A112 370 OHIO STATE UNIV COLUMBUS ELECTROSCIENCE LAB F/G 20/3
A UNIFORM ASYMPTOTIC RESULT FOR THE SCATTERING OF PLANE WAVES B--ETC(U)
MAR 76 P H PATHAK, W D BURNSIDE N62269-74-C-0788
UNCLASSIFIED ESL-3973-1 NL

1 of 1
AD A
112370

END
DATE
FILMED
4-82
DTIC

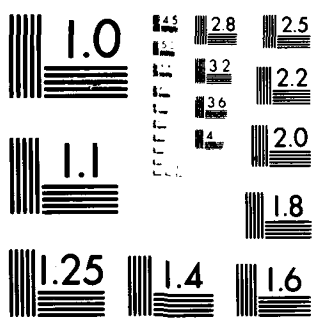

MICROCOPY RESOLUTION TEST CHART

PHOTOGRAPH THIS SHEET

DTIC ACCESSION NUMBER

A118 370

LEVEL II

INVENTORY

Ohio State Univ., Columbus
ElectroScience Lab.
A Uniform Asymptotic Result for the Scattering of Plane Waves by A Circular Cylinder.
Mar. 76

DOCUMENT IDENTIFICATION

Contract N62269-74-C-0788 Rept. No. ESL-3973-1

DISTRIBUTION STATEMENT A
Approved for public release;
Distribution Unlimited

DISTRIBUTION STATEMENT

ACCESSION FOR		
NTIS	GRA&I	☒
DTIC	TAB	☐
UNANNOUNCED		☐
JUSTIFICATION		

Per Ltr. on file
EL-88, Acc.# 82-0024(a)
BY Thru(d), Ltd 26 Jan.'82
DISTRIBUTION /
AVAILABILITY CODES

DIST	AVAIL AND/OR SPECIAL	
A		

DISTRIBUTION STAMP

DTIC
S ELECTE D
MAR 24 1982
D

DATE ACCESSIONED

82 03 08 149

DATE RECEIVED IN DTIC

PHOTOGRAPH THIS SHEET AND RETURN TO DTIC-DDA-2

DTIC FORM OCT 79 70A

DOCUMENT PROCESSING SHEET

UNCLASSIFIED

SECURITY CLASSIFICATION OF THIS PAGE (When Data Entered)

REPORT DOCUMENTATION PAGE		READ INSTRUCTIONS BEFORE COMPLETING FORM
1. REPORT NUMBER	2. GOVT ACCESSION NO.	3. RECIPIENT'S CATALOG NUMBER
4. TITLE (and Subtitle) A UNIFORM ASYMPTOTIC RESULT FOR THE SCATTERING OF PLANE WAVES BY A CIRCULAR CYLINDER		5. TYPE OF REPORT & PERIOD COVERED Final Report
		6. PERFORMING ORG. REPORT NUMBER ESL 3973-1
7. AUTHOR(s) P. H. Pathak and W. D. Burnside		8. CONTRACT OR GRANT NUMBER(s) N62269-74-C-0788
9. PERFORMING ORGANIZATION NAME AND ADDRESS The Ohio State University ElectroScience Laboratory, Department of Electrical Engineering, Columbus, Ohio 43212		10. PROGRAM ELEMENT, PROJECT, TASK AREA & WORK UNIT NUMBERS
11. CONTROLLING OFFICE NAME AND ADDRESS Department of the Navy Naval Air Development Center Warminster, Pennsylvania 18974		12. REPORT DATE March 1976
		13. NUMBER OF PAGES 63
14. MONITORING AGENCY NAME & ADDRESS (if different from Controlling Office)		15. SECURITY CLASS. (of this report) UNCLASSIFIED
		15a. DECLASSIFICATION/DOWNGRADING SCHEDULE

16. DISTRIBUTION STATEMENT (of this Report)

DISTRIBUTION STATEMENT A

Approved for public release; Distribution Unlimited

17. DISTRIBUTION STATEMENT (of the abstract entered in Block 20, if different from Report)

18. SUPPLEMENTARY NOTES

19. KEY WORDS (Continue on reverse side if necessary and identify by block number)

Circular Cylinder	Transition Region
Electromagnetic Scattering	Uniform Result
Geometrical Theory of Diffraction (GTD)	Off-Fuselage Aircraft Antenna

20. ABSTRACT (Continue on reverse side if necessary and identify by block number)

The canonical problem of plane wave scattering by a perfectly-conducting circular cylinder is analyzed, and a uniform asymptotic result is presented for the field within the transition regions adjacent to the shadow boundaries where the ordinary ray solutions fail. This result provides a finite and continuous total field across the shadow boundaries. Exterior to the transition regions it reduces to the GTD solution in terms of the surface diffracted and the geometric optical (incident and reflected) ray fields for the shadow

20.

and lit zones, respectively. The accuracy of this transition solution is confirmed by numerical comparison with the results obtained via an exact solution for the same canonical problem. The transition solution is in terms of well tabulated functions, and it is simple and accurate for engineering applications (e.g., in determining the fields of wing or tail mounted aircraft antennas).

TABLE OF CONTENTS

LIST OF ILLUSTRATIONS

LIST OF ILLUSTRATIONS (continued)

LIST OF ILLUSTRATIONS (continued)

I. INTRODUCTION

When the geometrical theory of diffraction (GTD) [1,2] is employed to analyze the problem of high frequency plane wave scattering by smooth convex surfaces, a modification of this method is required for analyzing the fields in the vicinity of the shadow boundaries associated with this problem. This modification of the GTD forms the subject of the present paper.

In the GTD analysis of the diffraction of waves by a smooth convex cylinder [3], the total field exterior to it is associated in a simple manner with the usual incident and reflected rays of geometrical optics together with the surface diffracted rays introduced by Keller. The geometric optical rays are present only in the lit (or illuminated) region, so that the surface diffracted rays alone account for the field in the shadow region (these surface diffracted rays are also present in the illuminated region if the cylinder cross-section is closed). However, pure ray optical field descriptions fail at and near shadow boundaries, and at caustics of ray systems; consequently, the GTD ray solution for the problem illustrated in Fig. 1 is valid in regions I and III, but it fails in regions II, IV, V, and VI. Region II constitutes the penumbral or transition region adjacent to the shadow boundary (SB). The angular extent of this transition region is

$O\left[2\left(\frac{2}{k\rho_g(Q_1)}\right)^{1/3}\right]$ where k refers to the wavenumber of the surrounding medium which is assumed here to be free space, and $\rho_g(Q_1)$ is the radius of curvature of the cylinder at the point of grazing incidence, i.e., at Q_1. Regions IV, V, and VI are usually referred to as the surface or caustic boundary layer regions. In shadow regions IV and V, the surface of the obstacle is a caustic of the surface diffracted rays; whereas, region VI is in the neighborhood of Q_1 which is a caustic of the reflected ray for grazing incidence. The mathematical representations for the field within the transition regions, the surface boundary layer regions, and also their common regions of overlap are complicated by the fact that they must change rapidly but smoothly from one form to another across these regions.

It is evident that the usefulness and versatility of the GTD solution is further enhanced if it can be modified within the region where it fails; such modifications may be achieved by introducing uniform solutions which not only remain valid in one or more of these regions, but which reduce to the conventional GTD results exterior to these regions.

The development of a simple, uniform solution which remains valid in region II that is exter'or to the urface boundary layer is considered in this paper. Th work motivated by the need

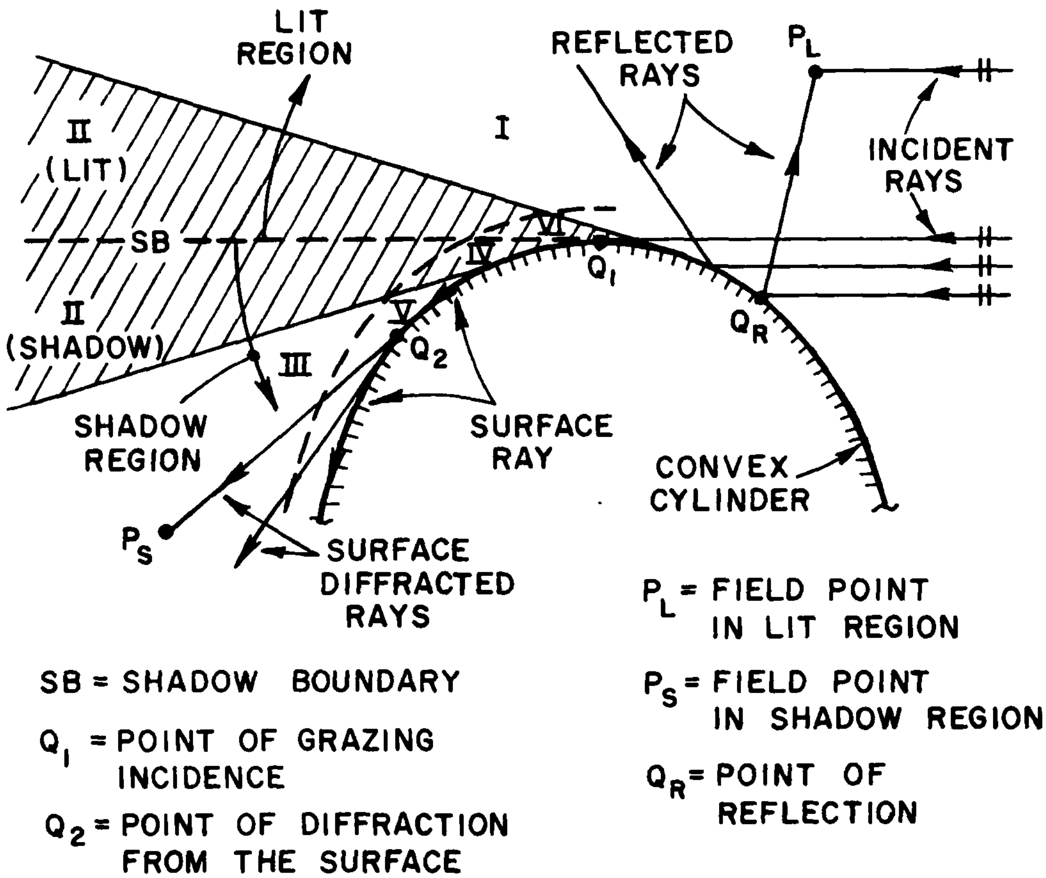

Fig. 1. Rays associated with the plane wave scattering by a smooth convex cylinder.

to analyze the radiation patterns of antennas mounted on the wings or tails of aircraft [4,5]. The radiation patterns of such antennas are significantly affected due to shadowing by the aircraft fuselage surface which is generally smooth and convex shaped. In many such wing or tail mounted aircraft antenna configurations, a knowledge of the field in the transition (or penumbral) region is essential for the purposes of antenna design. One can develop a solution for the transition region via an asymptotic high frequency analysis of a canonical problem which closely models the local geometry of the convex cylinder at Q_1.

In this paper, the canonical problem of plane wave scattering by a perfectly-conducting circular cylinder is solved by introducing certain asymptotic approximations, which are based on physical considerations, to obtain a uniform asymptotic result that is valid in the transition region exterior to the surface boundary layer. This uniform result yields a finite, continuous solution for the total field across the SB within the transition region. Exterior to this transition region, it reduces to the usual GTD solution in terms of surface diffracted and geometric optical ray fields for the shadow and lit zones, respectively. Furthermore, this result is in a form which is simple and convenient for engineering applications. Upon invoking the principle of the local character of the high frequency fields in the penumbra, one can systematically modify the uniform result for the circular cylinder to treat the electromagnetic scattering by arbitrary, smooth convex surfaces for both two- and three-dimensional problems. These extensions will be presented in detail in a separate paper.

The analysis of the canonical problem is indicated in section II. Numerical results based on this uniform-GTD analysis are compared in section III against the results obtained from an exact eigenfunction series solution for the same canonical problem where, it is seen that the present uniform result is accurate not only within, but also exterior to the transition region. A summary and discussion follows in section IV. Before proceeding with the analysis, the present work will be compared with the work of others on this subject.

The problem of asymptotically estimating the fields within the transition regions associated with the diffraction of waves by smooth, convex surfaces has had long standing interest, especially in connection with the theory of radio wave propagation around the earth. The fundamental work of Fock on this subject [6] appears to be the most significant; in particular, his analysis of the fields near a shadow boundary and within the Fresnel region of a diffracting spherical surface [7] is of direct relevance to the problem considered here. Other notable works which are also directly related to the present analysis are due to Wait and Conda [8], Logan and Yee [9,10], and Ivanov [11]. An extensive bibliography on various aspects of the problem of diffraction by a smooth, convex surface may be found in the papers by Logan [9,10], and Borovikov and Kinber [12]. Indeed, the present work draws upon the earlier, important contributions of Fock and Logan.

In Fock's analysis [7], the wave equation within the transition region is solved approximately via the method of parabolic equations; this solution is initially expressed in terms of a canonical integral introduced earlier by Fock [13a,b]. For observation points near the shadow boundary and the diffracting surface (but outside the surface boundary layer), this canonical integral is reduced by Fock to integrals which are functions of only a single parameter; in particular, the solution is expressed in terms of a Fresnel integral and a Pekeris-type integral [9,10], both of which are well tabulated.

Wait and Conda [8] analyze the field in the transition region scattered by a circular cylinder via an asymptotic evaluation of the radiation integral which employs the well-known Fock currents [13a] for this problem; their asymptotic solution near the shadow boundary is also given in terms of Fresnel and Pekeris integrals as done earlier by Fock [7]. In addition, the result given in [8] is valid not only near the surface (outside the surface boundary layer) as in [7], but also in the far zone. The analysis in [8] is an extension and generalization of the work of Goriainov [14].

The results in [7], [8], and [14] are quite accurate in the illuminated region very close to the SB, but in general they do not join smoothly with the geometrical optics field; whereas, the result presented here does reduce to the geometrical optics field in the illuminated region. Also, the present result is valid in both the near and far zone as in [8]; furthermore, exactly on the shadow boundary, it agrees with the results of [7], [8], and [14] which are accurate near the shadow boundary. Logan and Yee [10] give a result for the illuminated part of the transition region in terms of the canonical integral of Fock such that it reduces to the geometrical optics field far from the shadow boundary. This result appears to have been constructed by redefining certain parameters in Fock's canonical integral on an ad hoc basis.

Ivanov [11] analyzes the same canonical problem as in this paper via the method of parabolic equations; his solution which is valid in the transition and the surface boundary layer regions, and which reduces to the GTD solution outside the transition region, is also given in terms of an integral related to the canonical integral of Fock. The canonical Fock integral-type solutions [10,11] are complicated for numerical evaluation in the transition region except when the field point is either very close to the shadow boundary, or is on the surface; in these exceptional cases, they reduce to well tabulated integrals which are functions of only a single parameter.

On the other hand, using a somewhat less formal analytical procedure than the parabolic equation method employed in [7], [10], and [11], the present solution is given in terms of the well tabulated single parameter Fresnel and Pekeris integrals for the entire transition region (exterior to the surface boundary layer). In this sense, the present result indicates a simplification over the results in [7], [10], and [11], respectively, for field points outside the surface boundary layer; furthermore, this simplification is achieved without any apparent loss of accuracy as confirmed by the numerical calculations in section III.

II. ANALYTICAL DETAILS

An asymptotic high frequency analysis of the canonical problem of electromagnetic plane wave scattering by a perfectly-conducting circular cylinder in free space is presented in this section; both, the TE and the TM polarization cases are considered. The geometrical configuration of this canonical problem is illustrated in Fig. 2.

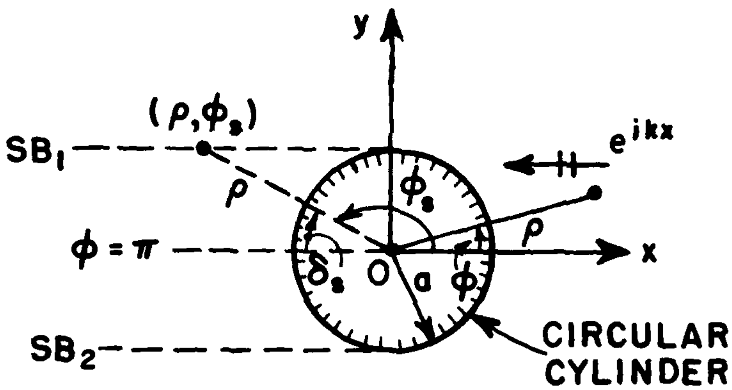

Fig. 2. Geometry of the canonical problem.

Let the incident plane wave field be denoted by U^i, and the scattered field by U^s; then, the total field is $U = U^i + U^s$ exterior to the cylinder. The total field U corresponds to a z-directed electric field if the excitation is TM_z polarized; whereas, it corresponds to a z-directed magnetic field if the excitation is TE_z polarized. The form of the incident field U^i is:

$$U^i = e^{ikx} \quad . \tag{1}$$

The total field, U satisfies the reduced wave equation

$$\left(\nabla^2 + k^2\right) U = 0 \quad , \tag{2}$$

where ∇^2 is the usual 2-D Laplacian operator in cylindrical coordinates (ρ,ϕ). The scattered field U^s satisfies the Sommerfeld radiation condition for an $e^{+i\omega t}$ time dependence (which is assumed and suppressed), and the total field $U(\rho,\phi)$ satisfies the following boundary conditions on the cylinder:

$$(3) \qquad Q\left[U(\rho,\phi)\right] = 0 \quad , \quad \text{at} \quad \rho = a; \; Q \equiv \begin{cases} 1, & \text{for the } TM_z \text{ case} \\ \frac{\partial}{\partial\rho}, & \text{for the } TE_z \text{ case.} \end{cases}$$

The solution to (2) subject to the radiation condition and (3) is [15]

$$(4a) \qquad U = -i \int_{-\infty-i\varepsilon}^{\infty-i\varepsilon} dv \left[J_v(k\rho) - \frac{Q\, J_v(ka)}{Q\, H_v^{(2)}(ka)} H_v^{(2)}(k\rho) \right] \cdot \frac{\cos v\,(\pi - |\phi|)}{\sin v\pi}\, e^{iv\frac{\pi}{2}} ,$$

or

$$(4b) \qquad U = -\frac{i}{2} \int_{-\infty-i\varepsilon}^{\infty-i\varepsilon} dv \left[H_v^{(1)}(k\rho) - \frac{Q\, H_v^{(1)}(ka)}{Q\, H_v^{(2)}(ka)} H_v^{(2)}(k\rho) \right] \cdot \frac{\cos v\,(\pi - |\phi|)}{\sin v\pi}\, e^{iv\frac{\pi}{2}} ,$$

with $\varepsilon>0$, and $\varepsilon \to 0$. The quantities J_v, $H_v^{(1),(2)}$ are the usual cylinder Bessel and Hankel functions. It is noted that $\mathrm{Im}(v)<0$ on the contour of integration in (4a) and (4b).

The above integral expressions for U may be rewritten by employing the decomposition

$$(5) \qquad \cos v(\pi - |\phi|) = e^{-iv\pi} \cos v\phi + i\, e^{-iv|\phi|} \sin v\pi \quad .$$

Thus, for large ka (i.e., ka>>1), one obtains

$$(6a) \qquad U \approx \int_{-\infty-i\varepsilon}^{\infty-i\varepsilon} dv \left[J_v(k\rho) - \frac{Q\, J_v(ka)}{Q\, H_v^{(2)}(ka)} H_v^{(2)}\,(k\rho) \right] e^{-iv[|\phi|-\frac{\pi}{2}]} ,$$

or

$$\text{(6b)} \qquad U \approx \frac{1}{2} \int_{-\infty-i\varepsilon}^{\infty-i\varepsilon} dv \left[H_v^{(1)}(k\rho) - \frac{Q\, H_v^{(1)}(ka)}{Q\, H_v^{(2)}(ka)} H_v^{(2)}(k\rho) \right] \cdot e^{-iv[|\phi| - \frac{\pi}{2}]} ,$$

with $0<|\phi|<\pi$. In going from (4) to (6) via (5), the terms containing $e^{iv\pi}$ cos $v\phi$ are discarded because they can be shown to correspond to the multiply encircling GTD surface ray modes which contribute negligibly for large ka. Within the transition region, $v \sim 0$ (ka) so that $J_v(ka)$ and $H_v^{(2)}(ka)$ become for large ka:

$$\text{(7a)} \qquad J_v(ka) \approx \frac{1}{m\sqrt{\pi}} V(m^{-1}[v-ka]) \quad ;$$

$$\text{(7b)} \qquad H_v^{\binom{(1)}{(2)}}(ka) \approx \mp \frac{i}{m\sqrt{\pi}} W_{\substack{1\\2}}(m^{-1}[v-ka])$$

where $m \equiv \left(\frac{ka}{2}\right)^{1/3}$, and the quantities V and $W_{\substack{1\\2}}$ are the Fock-type Airy functions* [9]. Introducing the change of variable $\tau = m^{-1}[v-ka]$ now allows one to express (6) in terms of (7) as:

$$\text{(8a)} \qquad U \approx m \int_{-\infty-i\varepsilon}^{\infty-i\varepsilon} d\tau \left[J_{v(\tau)}(k\rho) + i \frac{\tilde{Q}\, V(\tau)}{\tilde{Q}\, W_2(\tau)} \; H_{v(\tau)}^{(2)}(k\rho) \right] \cdot e^{-iv(\tau)\psi} ,$$

---

* $W_{1,2}(\tau) \equiv \frac{1}{\sqrt{\pi}} \int_{\Gamma_{1,2}} e^{\tau t - t^3/3}$; $2\, iV(\tau) \equiv W_1(\tau) - W_2(\tau)$. The contour Γ_1 runs from $\infty e^{-i\frac{2\pi}{3}}$ to $\infty - i\varepsilon$; whereas, Γ_2 is the complex conjugate of Γ_1.

or

$$(8b)\qquad U \approx \frac{m}{2} \int_{-\infty-i\varepsilon}^{\infty-i\varepsilon} d\tau \left[H_{v(\tau)}^{(1)}(k\rho) + \frac{\tilde{Q}\, W_1(\tau)}{\tilde{Q}\, W_2(\tau)}\; H_{v(\tau)}^{(2)}(k\rho) \right] e^{-iv(\tau)\psi} \quad ,$$

with

$$(8c)\qquad \tilde{Q} \equiv \begin{cases} 1, & \text{for the } TM_z \text{ case} \\ \frac{\partial}{\partial\tau}, & \text{for the } TE_z \text{ case} \end{cases} \quad .$$

Also, $v(\tau) = ka + m\,\tau$, $\psi \equiv |\phi| - \frac{\pi}{2}$, and $Im(\tau)<0$ in the integrands of (8a) and (8b).

The integral representations for U in (8) will next be asymptotically approximated for the shadowed zone of the transition region in part A of this section; whereas, the asymptotic approximation for U in the illuminated zone of the transition region will follow in part B.

A. Transition Region - Shadow Zone

One begins by rewriting (8) in a manner analogous to that done by Fock [7] in the decomposition of a canonical integral representing the solution of his parabolic equation for the problem of diffraction by a sphere; namely, U is written as a superposition of two integrals, one being the integral in (8a) over the contour from $0-i\varepsilon$ to $\infty-i\varepsilon$ (defined as contour C_2), and the other being the integral in (8b) over the contour from $-\infty-i\varepsilon$ to $0-i\varepsilon$ (defined as contour C_1). Thus,

$$(9)\qquad U \approx I_1 + I_2 \quad ,$$

where

$$(10a)\qquad I_1 \equiv m \int_{C_1+C_2} J_{v(\tau)}(k\rho)\, e^{-iv(\tau)\psi}\, d\tau - \frac{m}{2} \int_{C_1} H_{v(\tau)}^{(2)}(k\rho)\, e^{-iv(\tau)\psi}\, d\tau$$

and

$$\text{(10b)} \qquad I_2 \cong im \int_{C_2} \frac{\tilde{Q}\, V(\tau)}{\tilde{Q}\, W_2(\tau)} H^{(2)}_{v(\tau)}(k\rho)\, e^{-iv(\tau)\psi}\, d\tau + \frac{m}{2} \int_{C_1} \frac{\tilde{Q}\, W_1(\tau)}{\tilde{Q}\, W_2(\tau)} H^{(2)}_{v(\tau)}(k\rho)\, e^{-iv(\tau)\psi}\, d\tau \quad .$$

The contours C_1 and C_2 are shown in Figs. 3(a) and 3(b), respectively. One notes that I_1 is independent of the electrical properties of the cylinder; whereas, I_2 is strongly dependent on these properties.

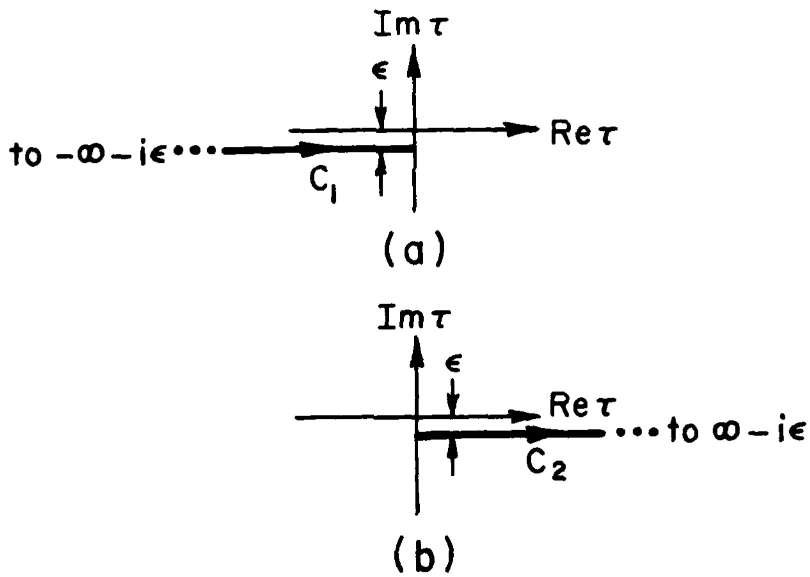

Fig. 3. Contours of integration for I_1 and I_2.

For the sake of definiteness, the fields in the transition region associated with the shadow boundary SB_1 will be analyzed here; in this case SB_1 exists within the domain $0<\phi<\pi$. The analysis for the transition region adjacent to SB_2 in the domain $-\pi<\phi<0$ is similar.

The first integral in I_1 can be solved by employing the usual integral representation for $J_v(k\rho)$, namely,

$$J_v(k\rho) = \frac{1}{2\pi} \int_{C_A+C_B} d\beta e^{-ik\rho \sin\beta + iv\beta} \quad ,$$

and interchanging the orders of integration to yield

$$(11) \qquad m \int_{C_1+C_2} J_{v(\tau)}(k\rho)\, e^{-iv(\tau)\psi}\, d\tau = e^{-ik\rho \sin\psi}$$

$$= e^{ik\rho\cos\phi}, \quad \text{for } 0<\phi<\pi \text{ and } |\psi|<\frac{\pi}{2} \quad .$$

Clearly, (11) is just the incident field. In deriving (11) use is also made of the following.

$$\frac{\delta(\psi-\beta)}{m} = \frac{1}{2\pi} \int_{C_1+C_2} d\tau\, e^{-im(\psi-\beta)\tau} \quad ,$$

where $\delta(\psi-\beta)$ is the Dirac delta function.

Next, the second term on the R.H.S. of (10a) may be re-expressed in terms of the standard integral representation for $H^{(2)}_{v(\tau)}(k\rho)$ as

$$- \frac{m}{2} \int_{C_1} H^{(2)}_{v(\tau)}(k\rho)\, e^{-iv(\tau)\psi}\, d\tau$$

$$= - \frac{m}{2} \int_{C_1} d\tau\, e^{-iv(\tau)\psi} \frac{1}{\pi} \int_{C_B} d\beta\, e^{-ik\rho\sin\beta + iv(\tau)\beta}$$

which for $\mathrm{Im}(\tau) < 0$ reduces to

(12) $\quad -\frac{m}{2}\int_{C_1} H_{v(\tau)}^{(2)}(k\rho)\, e^{-iv(\tau)\psi}\, d\tau = \frac{e^{-ika\,\psi}}{2\pi i}\int_{C_B} d\beta\, \frac{e^{-ik\rho\,[\sin\beta - \frac{a}{\rho}\beta]}}{\psi - \beta}$;

with $\quad \psi = \phi - \frac{\pi}{2}$, $|\psi|<\frac{\pi}{2}$ for $0<\phi<\pi$.

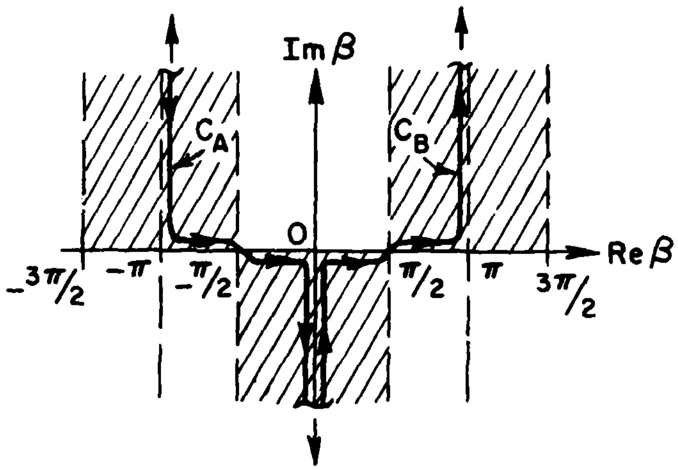

Fig. 4. Contours of integration for Bessel functions.

The contours of integration C_A and C_B occurring in the definitions of $J_v(k\rho)$ and $H_v^{(2)}(k\rho)$ are indicated in Fig. 4. The integrand on the R.H.S of (12) has a saddle point at $\beta = \beta_s$, where $\beta_s = \cos^{-1}\frac{a}{\rho}$. Since β_s is a constant for fixed values of ρ and a, it is conveniently determined by setting $\phi = \phi_s$ (for which the observation point is on SB_1); consequently, $\beta_s = \frac{\pi}{2} - \delta_s = \phi_s - \frac{\pi}{2}$, as shown in Fig. 2. Also, the integrand in (12) has a pole at $\beta = \beta_p$, where $\beta_p = \psi = \phi - \frac{\pi}{2}$. Let $\theta \equiv \psi - \beta_s$, then

(13) $\qquad \theta \equiv \psi - \beta_s = \beta_p - \beta_s = \phi - \phi_s \qquad .$

When $\phi>\phi_S$, the field point is in the shadow region; therefore, it follows that $\beta_p>\beta_s$ and $\theta>0$ in the shadow region. The integral on the R.H.S. of (12) can be evaluated via the method of steepest descent; hence, this integral over the countour C_B may be changed to an integral along the steepest descen path (SDP) through the saddle point β_S as indicated in Fig. 5. However, in the process of deforming the contour from C_B to SDP, the pole at β_p is crossed; it is therefore necessary to include it's residue in evaluating (12).

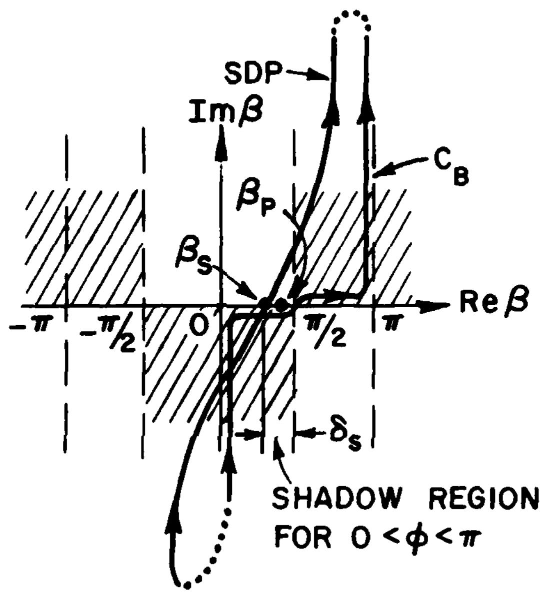

Fig. 5. Location of β_S, β_p and SDP for the shadow region analysis.

The integral in (12) now becomes:

$$(14)\qquad \frac{e^{-ika\psi}}{2\pi i}\int_{C_B} d\beta\,\frac{e^{-ik\rho[\sin\beta-\frac{a}{\rho}\beta]}}{\psi-\beta}$$

$$= -e^{ik\rho\cos\phi}\,H(\phi-\phi_s) - \frac{e^{-ika\psi}}{2\pi i}\int_{SDP} d\beta\,\frac{e^{-ik\rho[\sin\beta-\frac{a}{\rho}\beta]}}{\beta-\psi}$$

where the first term on the R.H.S. of (14) is the residue at β_p, and $H(\phi-\phi_s)$ is the unit step function:

$$(15) \qquad H(\phi-\phi_s) \equiv \begin{cases} 0 & , \phi < \phi_s \quad \text{(lit region)} \\ 1 & , \phi > \phi_s \quad \text{(shadow region)} \end{cases}$$

Therefore, the first term on the R.H.S. of (14) exactly cancels the incident field corresponding to (11) in the shadow. Approximating $[\sin\beta - \frac{a}{\rho}\beta]$ in the exponent of the integrand on the R.H.S of (14) by its three term Taylor expansion about the saddle point β_s gives:

$$(16) \qquad -\frac{e^{-ika\psi}}{2\pi i} \int_{SDP} d\beta \, \frac{e^{-ik\rho[\sin\beta - \frac{a}{\rho}\beta]}}{\beta - \psi}$$

$$\approx -\frac{e^{-iks - ika\theta}}{2\pi i} \int_{SDP} d\beta \, \frac{e^{iks[\frac{1}{2}(\beta-\beta_s)^2]}}{\beta - \beta_p} \quad ,$$

where

$$(17) \qquad s^2 \equiv \rho^2 - a^2 \quad .$$

The integral on the R.H.S of (16) is now in a form which can be readily evaluated asymptotically for large ks by the Pauli-Clemnow modified method of steepest descent [16,17] for a pole close to a saddle point, to yield the following result for the integral in (12).

$$(18) \qquad -\frac{m}{2} \int_{C_1} H^{(2)}_{v(\tau)}(k\rho)\, e^{-iv(\tau)\psi}\, d\tau \sim -e^{ik\rho\cos\phi} H(\phi-\phi_s)$$

$$+ \frac{e^{-i\frac{\pi}{4}}}{\sqrt{2\pi k}} \, \frac{e^{-ika\theta}}{\theta} \, F[kL\tilde{a}] \, \frac{e^{-iks}}{\sqrt{s}} \quad ,$$

where the function $F[kL\tilde{a}]$ involves a Fresnel integral [17,18].

$$F[kL\tilde{a}] = 2\,i\,\sqrt{kL\tilde{a}}\; e^{ikL\tilde{a}} \int_{\sqrt{kL\tilde{a}}}^{\infty} e^{-i\tau^2}\, d\tau \quad ; \tag{19}$$

in which one takes the positive branch of $\sqrt{kL\tilde{a}}$.

The distance parameter L in (19) for this case is

$$L = s \quad ; \tag{20}$$

also, the quantity $\tilde{a}$ in the argument $kL\tilde{a}$ of F is

$$\tilde{a} = \frac{\theta^2}{2} \quad . \tag{21}$$

It is noted that kL is always the large parameter in this asymptotic solution involving $F[kL\tilde{a}]$. Plots of the magnitude and phase of the function $F[kL\tilde{a}]$ versus $kL\tilde{a}$ are illustrated in Fig. 6. The physical significance of the geometric quantities θ and s which appear in (18) is evident from Fig. 7. Combining (11) and (18), one obtains the following asymptotic result for I_1.

$$I_1 \sim e^{ik\rho\cos\phi} + \left\{ - e^{ik\rho\cos\phi}\, H(\phi-\phi_s) + \frac{e^{-i\frac{\pi}{4}}}{\sqrt{2\pi k}}\, \frac{e^{-ika\theta}}{\theta}\, F[kL\tilde{a}]\, \frac{e^{-iks}}{\sqrt{s}} \right\} ; \quad \phi > \phi_s,\ 0<\phi<\pi. \tag{22a}$$

Or,

$$I_1 \sim \frac{e^{-i\frac{\pi}{4}}}{\sqrt{2\pi k}}\, \frac{e^{-ika\,\theta}}{\theta}\, F[kL\tilde{a}]\, \frac{e^{-iks}}{\sqrt{s}} \quad ; \quad \phi>\phi_s,\ 0<\phi<\pi. \tag{22b}$$

Turning next to the evaluation of I_2 in (10b), it is observed that the integrals in (10b) can be simplified if the $H^{(2)}_{v(\tau)}(k\rho)$ terms appearing therein are replaced by the well known Debye approximation which is valid for $v(\tau)<k\rho$ and $v(\tau)$ large. Since $v(\tau) = ka + m\tau$ and $v(\tau) \sim O(ka)$ in the transition region, the major contribution to the integrals in (10b) occur for τ small. In this

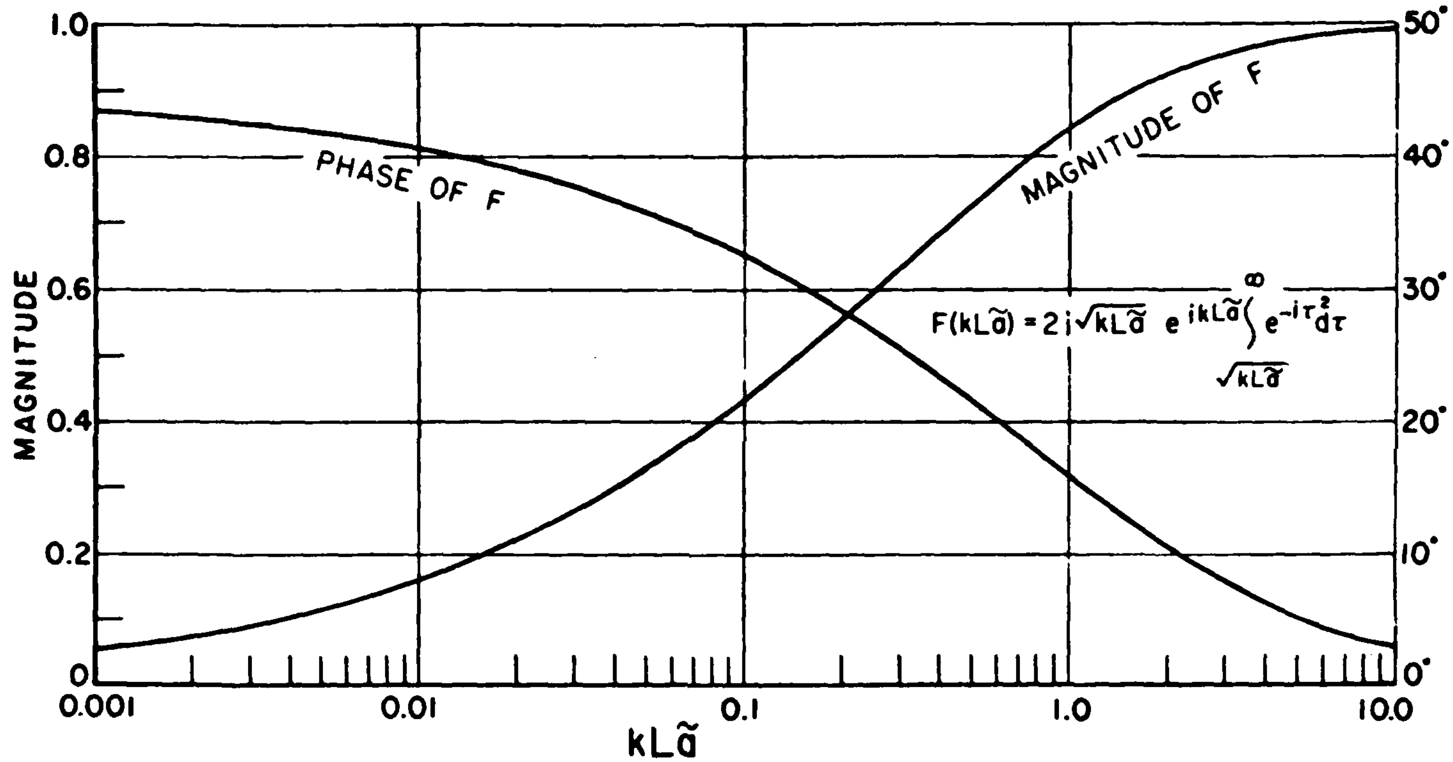

Fig. 6. Transition region correction factor $F(kL\tilde{a})$ (the positive branch of $\sqrt{kL\tilde{a}}$ is taken).

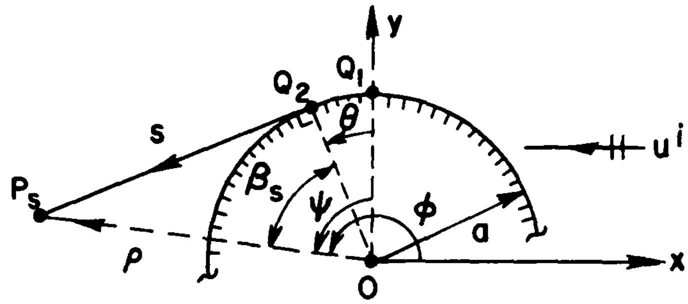

$$s^2 = \rho^2 - a^2$$

$$\beta_s = \cos^{-1}\frac{a}{\rho}$$

$$\theta = \psi - \beta_s > 0$$

Fig. 7. Geometrical parameters for the shadow region.

case, $\frac{v(\tau)}{k\rho} = \frac{a}{\rho} + \tau\frac{m}{k\rho} \approx \frac{a}{\rho}$ so that $v(\tau) < k\rho$ is satisfied, and the Debye approximation may be employed for $H^{(2)}_{v(\tau)}(k\rho)$ as follows.

$$H^{(2)}_{v(\tau)}(k\rho) \sim \sqrt{\frac{2}{\pi k\rho \sin\gamma}}\; e^{-ik\rho\sin\gamma + iv(\tau)\gamma + i\frac{\pi}{4}} \quad ;$$

with

$$v(\tau) < k\rho, \text{ and } \cos\gamma = \frac{v}{k\rho} \quad .$$

When $v(\tau) \sim O(ka)$, $\cos\gamma \approx \frac{a}{\rho}$ so that $\gamma \approx \beta_s$, and $\sin\gamma = \frac{\left[(k\rho)^2 - (v(\tau))^2\right]^{1/2}}{k\rho} \approx \frac{k\left[\rho^2 - a^2\right]^{1/2}}{k\rho} = \frac{s}{\rho}$. Incorporating these simplifications in the Debye approximation yields:

$$H^{(2)}_{v(\tau)}(k\rho) \sim \sqrt{\frac{2}{\pi ks}}\; e^{-iks + i\frac{\pi}{4}}\; e^{i(ka + m\tau)\beta_s} \quad . \tag{23}$$

Next, incorporating (23), and the relation $\tilde{Q}\, W_1(\tau) = \tilde{Q}\, W_2(\tau) + 2\, i\tilde{Q}\, V(\tau)$ into the integrals in (10b) leads to the following expression for I_2:

$$\text{(24a)} \qquad I_2 \approx \sqrt{\frac{2}{ks}}\, e^{-iks\,-\,ika\theta}\, m\, \frac{e^{i\frac{\pi}{4}}}{\sqrt{\pi}} \left[\frac{1}{2} \int_{C_1} e^{-im\tau\theta}\, d\tau + i \int_{C_1+C_2} \frac{\tilde{Q}\, V(\tau)}{\tilde{Q}\, W_2(\tau)}\, e^{-im\tau\theta}\, d\tau \right] .$$

I_2 can be further simplified in a straight forward manner to obtain:

$$\text{(24b)} \qquad I_2 \sim -\frac{e^{-i\frac{\pi}{4}}}{\sqrt{2\pi k}}\, \frac{e^{-ika\,\theta}}{\theta}\, \frac{e^{-iks}}{\sqrt{s}} - m\sqrt{\frac{2}{k}}\, e^{-ika\,\theta}\, \hat{P}_{\substack{s\\h}}(\xi)\, \frac{e^{-iks}}{\sqrt{s}}$$

where $\hat{P}_{\substack{s\\h}}(\xi)$ is the Pekeris caret function [9] defined by:

$$\text{(25)} \qquad \hat{P}_{\substack{s\\h}}(\xi) \equiv \frac{e^{-i\frac{\pi}{4}}}{\sqrt{\pi}} \int_{-\infty}^{\infty} \frac{\tilde{Q}\, V(\tau)}{\tilde{Q}\, W_2(\tau)}\, e^{-i\xi\tau}\, d\tau \quad ,$$

and the parameter ξ is defined by

$$\text{(26)} \qquad \xi \equiv m\,\theta \qquad (\xi > 0 \text{ in the shadow region}).$$

The subscript s on $\hat{P}_s$ is used to denote the TM_z (or acoustical soft) case; whereas, the subscript h on $\hat{P}_h$ denotes the TE_z (or accoustical hard) case. Values of $\hat{P}_{\substack{s\\h}}(\xi)$ versus ξ are presented in Fig. 8 in terms of related functions $p^*(\xi)$ and $q^*(\xi)$.

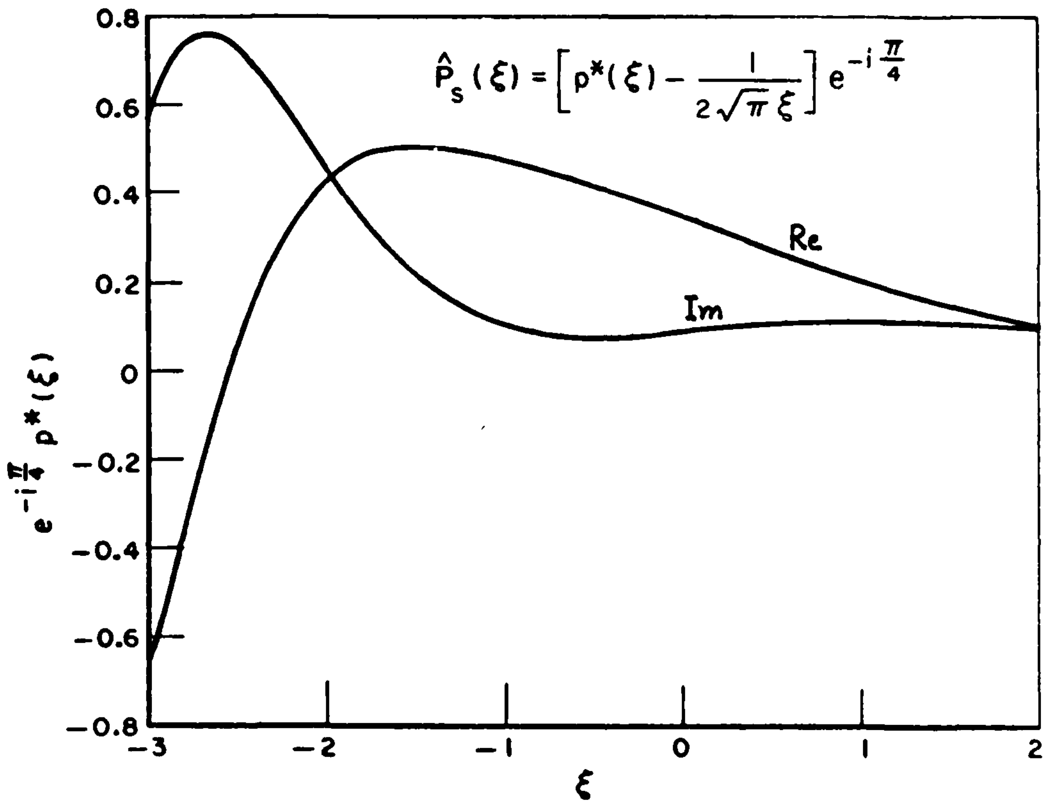

Fig. 8(a). Plot of $e^{-i\pi/4}p^*(\xi)$ versus ξ based on Logan's tabulated data [9] for $p(\xi)$.

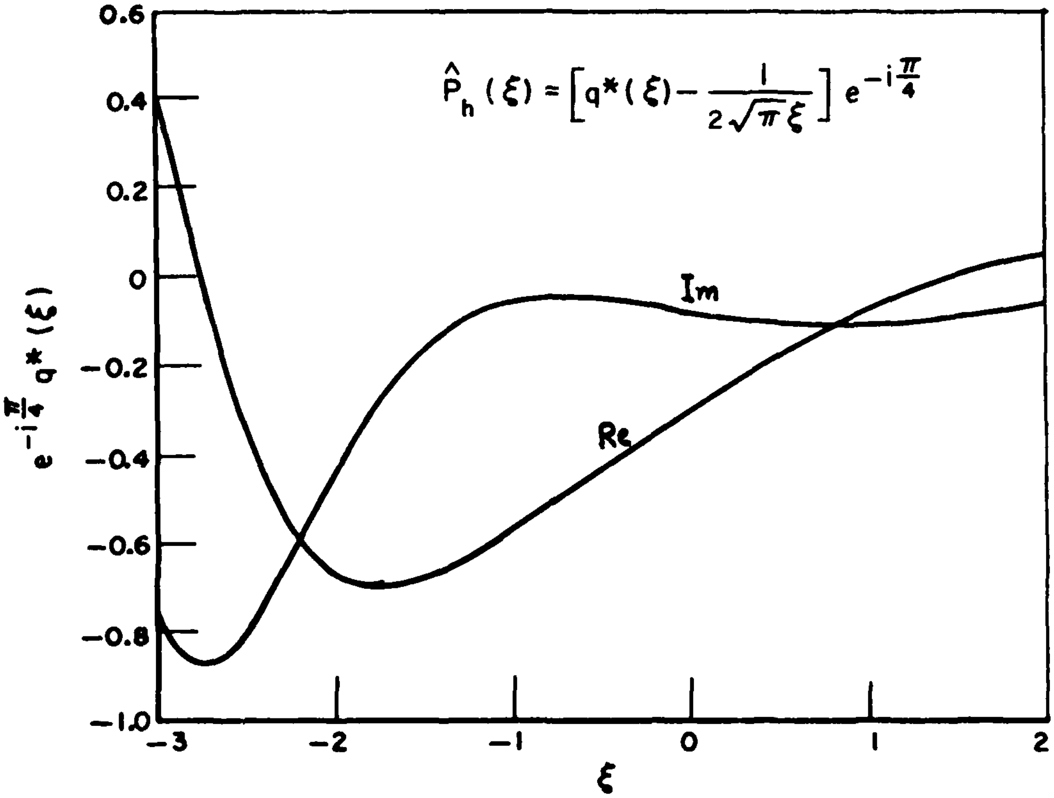

Fig. 8(b). Plot of $e^{-i\pi/4}q^*(\xi)$ versus ξ based on Logan's tabulated data [9] for $q(\xi)$.

Combining the results of (22b) and (24b), one obtains the following asymptotic expression for U (of Eq. (9)) which is valid at the observation point P_s in the shadowed portion of the transition region.

$$(27) \qquad U(P_s) \sim -\frac{e^{-i\frac{\pi}{4}}}{\sqrt{2\pi k}} \frac{e^{-ika\theta}}{\theta} \left\{ 1 - F[kL\tilde{a}] \right\} \frac{e^{-iks}}{\sqrt{s}}$$

$$- m\sqrt{\frac{2}{k}}\, e^{-ika\theta}\, \hat{P}_{\substack{s\\h}}(\xi) \frac{e^{-iks}}{\sqrt{s}} \quad ; \quad \theta > 0,\ \phi > \phi_s,\ \xi > 0.$$

The above result for U may be interpreted geometrically as a field which after being launched by the incident wave at Q_1 propagates along the path $Q_1Q_2P_s$ to the field point P_s, as indicated in Fig. 7. Q_1 and Q_2 are tangent points which correspond to the point of grazing incidence on the cylinder, and the point of tangential shedding of the diffracted wave from the surface, respectively.

One may now examine the result of directly extending the analysis presented above to lit region. In the lit region, $\phi<\phi_s$ and $\beta_p<\beta_s$ as indicated in Fig. 9 (note: Fig. 5 shows $\beta_p>\beta_s$ in shadow region). Consequently, $H(\phi-\phi_s) = 0$; also, $\theta<0$ ($\xi<0$) for $\phi<\phi_s$, and the field U at the point P_L in the lit region becomes via (22a) and (24b):

$$(28) \qquad U(P_L) \sim e^{ik\rho\cos\phi} - \frac{e^{-i\frac{\pi}{4}}}{\sqrt{2\pi k}} \frac{e^{-ika\theta}}{\theta} \left\{ 1 - F[kL\tilde{a}] \right\} \frac{e^{-iks}}{\sqrt{s}}$$

$$- m\sqrt{\frac{2}{k}}\, e^{-ika\theta}\, \hat{P}_{\substack{s\\h}}(\xi) \frac{e^{-iks}}{\sqrt{s}} \quad ; \quad \phi<\phi_s;\ \theta<0;\ \xi<0.$$

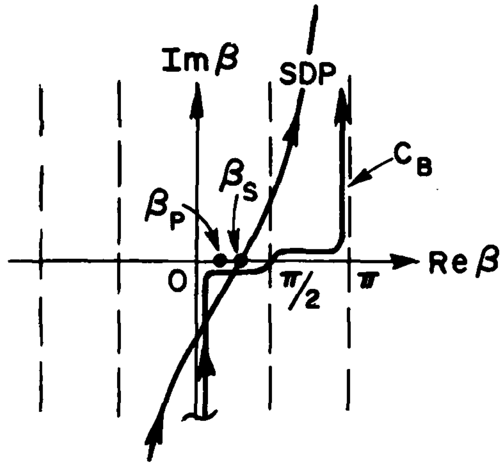

Fig. 9. Location of β_s, β_p and SDP for the lit region.

Equations (27) and (28) may be represented compactly in a single expression as follows:

$$(29) \qquad U(P) \sim e^{ik\rho\cos\phi}\, H(-\theta) - \frac{e^{-i\frac{\pi}{4}}}{\sqrt{2\pi k}}\, \frac{e^{-ika\theta}}{\theta} \left\{ 1 - F\left[\frac{kL\xi^2}{2m^2}\right]\right\} \frac{e^{-iks}}{\sqrt{s}}$$

$$- m\sqrt{\frac{2}{k}}\, e^{-ika\theta}\, \hat{P}_{\substack{s\\h}}(\xi)\, \frac{e^{-iks}}{\sqrt{s}}$$

with: $kL\tilde{a} = kL\frac{\xi^2}{m^2}$, $\xi = m\theta$, $L = s$; also,

$P = P_L$, for $\xi<0$, $\theta<0$, and $\phi<\phi_s$ (in the lit region),
$P = P_s$, for $\xi>0$, $\theta>0$, and $\phi>\phi_s$ (in the shadow region),

$$H(-\theta) = \begin{cases} 1, & \theta<0 \text{ for } P = P_L \\ 0, & \theta>0 \text{ for } P = P_s \end{cases} .$$

The first term on the RHS of (28) and (29) is just the incident field $U^i(P)$. The geometrical interpretation for the propagation of the field U in the lit region is presented in Fig. 10; this interpretation is simply an extension of that in Fig. 7 for the shadow region; more will be said about this later.

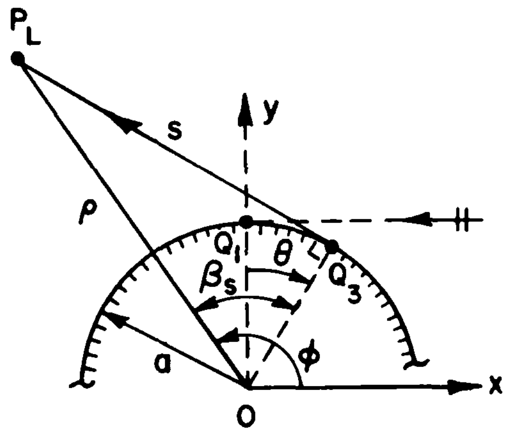

$$s^2 = \rho^2 - a^2 \; ; \quad \beta_s = \cos^{-1} \frac{a}{\rho}$$

$$\theta = \psi - \beta_s < 0$$

Fig. 10. Geometrical parameters for the lit region.

The result in (29) will be shown to be finite and continuous across SB_1. As one approaches SB_1, $\phi \to \phi_s$ and $\theta \to 0$; hence, $\tilde{a} = \frac{\theta^2}{2} \to 0$ and $\xi \to 0$. The limiting forms of $F[kL\tilde{a}]$ and $\hat{P}_{\substack{s\\h}}(\xi)$ as θ, $\xi \to 0$ are [18,19]:

$$\text{(30a)} \qquad F[kL\tilde{a}] \approx \left(\left| \sqrt{\pi kL\tilde{a}} \right| - 2\, kL\tilde{a}\, e^{i\frac{\pi}{4}} \right) e^{i(\frac{\pi}{4} + kL\tilde{a})} \quad ,$$

for a given kL as $\tilde{a}\to 0$; and

$$\text{(30b)} \qquad \hat{P}_{\substack{s\\h}}(\xi) \equiv \left[\begin{Bmatrix} p^*(\xi) \\ q^*(\xi) \end{Bmatrix} - \frac{1}{2\sqrt{\pi}\xi}\right] e^{-i\frac{\pi}{4}} \to \quad - \frac{e^{-i\frac{\pi}{4}}}{2\sqrt{\pi}\xi}$$

+ (small contribution from p* or q* which is continuous w.r.t. ξ), as $\xi\to 0$.

(Note: the $p^*(\xi)e^{-i\frac{\pi}{4}}$ and $q^*(\xi)e^{-i\frac{\pi}{4}}$ functions are plotted in Fig. 8.)

Employing the above limiting forms of (30a; 30b) in (29) as θ, $\xi\to 0$ from both, the lit (θ, $\xi<0$) and shadow (θ, $\xi>0$) directions, it is easily verified that U in (29) is finite and continuous across SB_1; in fact, exactly at SB_1, U(P) becomes:

$$\text{(31)} \qquad U(P)\Big|_{SB_1} \sim \frac{1}{2}e^{ikx} - m\sqrt{\frac{2}{k}}\; e^{-i\frac{\pi}{4}} \begin{Bmatrix} p^*(0) \\ q^*(0) \end{Bmatrix} \frac{e^{ikx}}{|\sqrt{x}|} \quad ;$$

$$\text{for} \begin{Bmatrix} TM_z \text{ case} \\ TE_z \text{ case} \end{Bmatrix},$$

where $x = \rho\cos\phi_s = -s$ along SB_1 (a similar result holds for SB_2). The first term on the R.H.S. of (31) is simply one-half the incident field on the shadow boundary as in the diffraction by a half-plane; the second term is dependent on surface properties.

Turning now to the evaluation of the field in the shadow region, but away from SB_1 and exterior to the transition region (i.e., in region III of Fig. 1), one notes that $F[kL\tilde{a}]\to 1$ since θ, and hence $kL\tilde{a}$ become large in this case (see Fig. 6); only the term containing $P_{\substack{s\\h}}(\xi)$ in (29) now remains significant. Far from SB_1 the integral for $\hat{P}_{\substack{s\\h}}(\xi)$ in (25) may be replaced by a rapidly convergent residue series [9]:

$$(32)\qquad \hat{P}_{\substack{s\\h}}(\xi)\Big|_{\xi>0} = \begin{cases} -\dfrac{e^{-i\frac{\pi}{4}}}{\sqrt{\pi}} \displaystyle\sum_n \dfrac{e^{i\frac{\pi}{6}}\, e^{\xi q_n e^{-i\frac{5\pi}{6}}}}{2[Ai'(-q_n)]^2} & \text{,for } \mathcal{Q}=1 \text{ or } TM_z \text{ case} \\[2ex] -\dfrac{e^{-i\frac{\pi}{4}}}{\sqrt{\pi}} \displaystyle\sum_n \dfrac{e^{i\frac{\pi}{6}}\, e^{\xi \bar{q}_n e^{-i\frac{5\pi}{6}}}}{2[Ai(-\bar{q}_n)]^2\, \bar{q}_n} & \text{, for } \mathcal{Q}=\dfrac{\partial}{\partial\tau} \text{ or } TE_z \text{ case} \end{cases}$$

where Ai is the Miller-type Airy function* (which is related to the Fock-type Airy function [9]), and Ai' is it's derivative with respect to the argument. The q_n and $\bar{q}_n$ are roots of $Ai(-q_n) = 0$ and $Ai'(-\bar{q}_n) = 0$, respectively for $n = 1,2,3, \cdots$. These roots are tabulated in [9].

When the above residue series representation of (32) is employed in $P_{\substack{s\\h}}(\xi)$ of (29) for $kL\tilde{a}>10$ (i.e., as $F[kL\tilde{a}]\to 1$), it can be readily shown that (29) reduces to

$$(33)\qquad U(P_s) \sim U^i(Q_1)\left[\sum_n D_n^{\substack{s\\h}}(Q_1)\, e^{-ika\theta - \alpha_n^{\substack{s\\h}} a\theta}\, D_n^{\substack{s\\h}}(Q_2)\right] \frac{e^{-iks}}{\sqrt{s}} \;,$$

where $D_n^{\substack{s\\h}}$ and $\alpha_n^{\substack{s\\h}}$ are the Keller diffraction and attenuation coefficients [3] associated with the GTD surface ray modes, respectively, with $D_n^{\substack{s\\h}}(Q_1) = D_n^{\substack{s\\h}}(Q_2)$ for the circular cylinder. The superscripts in $D_n^{\substack{s\\h}}$ and $\alpha_n^{\substack{s\\h}}$ correspond exactly to the subscripts in $\hat{P}_{\substack{s\\h}}(\xi)$ for the two polarizations; also, the subscript n denotes the

---

$$*\ Ai(\tau) = V(\tau)/\sqrt{\pi} = \frac{1}{2\pi}\int_{-\infty}^{\infty} dt\; e^{-i(\tau t + t^3/3)}\ ;\ Ai'(\tau) = \frac{dAi(\tau)}{d\tau}\ .$$

surface ray modal index. The $U^i(Q_1)$ in (33) represents the incident field at Q_1 and is unity for this problem. Thus, in the deep shadow (i.e., corresponding to region III of Fig. 1), (29) reduces to the GTD surface diffracted ray field given by (33) as it should. The geometrical interpretation of the GTD field in (33) is, of course, identical to that in Fig. 7. For the sake of convenience, and completeness, the diffraction and attenuation coefficients in (33) are listed below.

$$\left[D_n^s\right]^2 \sim \frac{\sqrt{\pi}\, 2^{-5/6}\, \rho_g^{1/3}\, e^{-i\pi/12}}{K^{1/6}\left[Ai'(-q_n)\right]^2} \; ; \; \alpha_n^s \sim \frac{q_n}{\rho_g}\, e^{i\pi/6}\left(\frac{k\rho_g}{2}\right)^{1/3}$$

$$\left[D_n^h\right]^2 \sim \frac{\sqrt{\pi}\, 2^{-5/6}\, \rho_g^{1/3}\, e^{-i\pi/12}}{K^{1/6}\, \bar{q}_n \left[Ai(-\bar{q}_n)\right]^2} \; ; \; \alpha_n^h \sim \frac{\bar{q}_n}{\rho_g}\, e^{i\pi/6}\left(\frac{k\rho_g}{2}\right)^{1/3}$$

B. Transition Region - Iluminated Zone

Although the result in (29) is applicable to both the shadow and lit portions of the transition region, it does not reduce to the geometrical optics field in the lit region. Consequently, the result in (29) is expected to be accurate in the shadow region both near and far from SB_1; whereas, it is expected to be accurate only for θ small in the lit region (ξ, $\theta<0$). This deficiency of (29) for the lit region where θ is not small is briefly discussed, and an improved solution which overcomes this difficulty is presented.

For the shadowed part of the transition region, the result in (29) has the geometrical interpretation illustrated in Fig. 7 which is identical to the GTD surface diffracted ray picture as shown in Fig. 1; consequently, it is not too surprising that Eq. (29) does indeed reduce exactly to the GTD solution of Eq. (33) in the deep shadow. On the other hand, the geometrical interpretation of the scattered field in (29) for the lit region ($\theta<0$) is illustrated in Fig. 10 which constitutes a direct generalization of the interpretation in Fig. 7 (for $\theta>0$); clearly, the ray geometry in Fig. 10 is in disagreement with the geometrical optics reflected ray picture of Fig. 11 which is known to be valid in the lit region. Consequently, one might anticipate the failure of Eq. (29) to reduce to the geometrical optics field in the lit region as a result of the differences between the scattered field propagation mechanisms of Figs. 10 and 11.

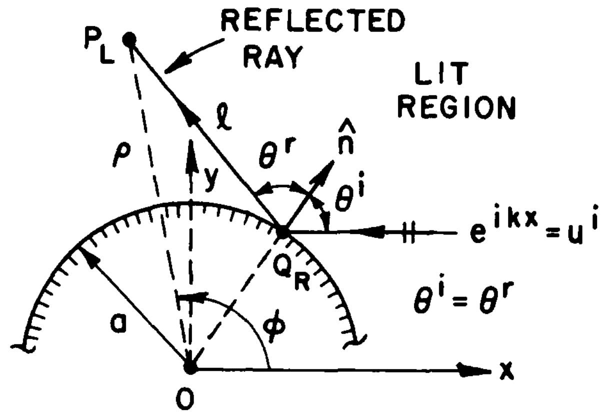

Fig. 11. Reflected ray system.

From Fig. 10, it is observed that the scattered field at P_L traverses the path $Q_1Q_3P_L$ after being launched by the incident wave at Q_1. This interpretation requires the field to propagate backward from Q_1 to Q_3 and then shed to P_L along the backward tangent at Q_3; in contrast, the geometric optical reflected ray trajectory touches the surface only at Q_R as in Fig. 11. The paths in Figs. 7 and 11 satisfy the extended Fermat's principle; whereas, the ray path in Fig. 10 does not. The inability of Eq. (29) to reduce to the geometrical optics field may be explained on the basis of the approximation in (23) for the Hankel function $H^{(2)}_{\nu(\tau)}(k\rho)$ which is employed in the evaluation of the transition region field; more will be said about this shortly.

For the sake of completeness, the behavior of Eq. (29) in the deep lit region is examined. As before, $F[kL\hat{a}] \to 1$ as the field point moves away from SB_1 in both the lit and shadow zones, thereby leaving the term containing $P_{s \atop h}(\xi)$ as the dominant contributor to the scattered field. Hence, in the lit region far from SB_1 where $\xi \ll 0$, Eq. (29) reduces to

$$(34) \qquad U(P_L) \sim e^{ik\rho\cos\phi} H(-\theta) - m\sqrt{\frac{2}{k}}\; e^{-ika\theta}\, \hat{P}_{\substack{s\\h}}(\xi)\, \frac{e^{-iks}}{\sqrt{s}} \quad ,$$

$$\theta<0,\ \xi<<0.$$

When $\xi<<0$, $\hat{P}_{\substack{s\\h}}(\xi)$ has the following asymptotic value [9]

$$(35) \qquad \hat{P}_{\substack{s\\h}}(\xi) \sim \pm\frac{\sqrt{-\xi}}{2}\, e^{i\frac{\xi^3}{12}}\,[1 + O(\xi^{-3})] \quad ; \quad \xi<<0.$$

Incorporating (35) into (34), one arrives at the following

$$(36) \qquad U(P_L) \sim U^i(P_L) \mp \sqrt{\frac{a|\theta|}{4}}\; e^{ika[|\theta| - \frac{|\theta|^3}{24}]}\; \frac{e^{-iks}}{\sqrt{s}}$$

$$\text{for} \begin{Bmatrix} TM_z \\ TE_z \end{Bmatrix} \text{case} \qquad \text{when } \xi<<0.$$

On the other hand, the geometrical optics field represents the correct asymptotic result far from SB_1 in the lit region, and its field associated with the incident and reflected rays is well known to be

$$(37) \qquad U(P_L) \sim U^i(P_L) \mp U^i(Q_R)\sqrt{\frac{\rho_r}{\rho_r + \ell}}\; e^{-ik\ell}$$

where $U^i(P_L) = e^{ik\rho\cos\phi}$ and $U^i(Q_R) = e^{ika\cos\theta^i}$ (see Fig. 11). The first term on the RHS of Eq. (37) is the incident field at P_L, and the second term denotes the reflected ray field. Q_R is the point of reflection on the surface as shown in Fig. 11, and the $\{\mp\}$ sign in front of $U^i(Q_R)$ denotes the value of the surface reflection coefficient at Q_R for the $\begin{Bmatrix} TE_z \\ TM_z \end{Bmatrix}$ case. The spatial distance ℓ is given by $\ell = Q_RP_L$; whereas, the caustic distance ρ_r associated with the reflected field is

$$\rho_r = \frac{a \cos \theta^i}{2} \quad . \tag{38}$$

The quantities ℓ and θ^i are also shown in Fig. 11.

One notes that Eq. (36) and Eq. (37) are nearly equal only for θ very small. In general, therefore, the result of Eq. (29) fails to reduce the geometrical optics result when $\xi<<0$ (this failure is similar to that which occurs in the results of [7], [8], and [14]); consequently, in order to overcome this limitation, one must employ an approximation for $H^{(2)}_{v(\tau)}(k\rho)$ in the lit region which is different from that in (23), and which leads to a geometrical interpretation for the scattered field in the lit region which is in agreement with the reflected ray geometry of Fig. 11.

The approximation of $H^{(2)}_{v(\tau)}(k\rho)$ in (23) is valid for $v(\tau) \sim O(ka)$; the condition $v(\tau) \sim O(ka)$ holds in the transition region near SB_1 and also in the deep shadow zone where only the first couple of GTD surface ray modes (corresponding to n = 1, 2, etc., in (32) and (33)) are necessary to describe the field accurately; whereas, deep in the lit region $v(\tau)$ can be significantly different from ka. Thus, Eq. (23) leads to the result of Eq. (29) which is accurate in the shadow region, but it is not expected to be accurate in the lit region if the field point is not close to SB_1.

The Fock-type Airy terms $\tilde{Q}\, V(\tau)$, and $\tilde{Q}\, W_{\genfrac{}{}{0pt}{}{1}{2}}(\tau)$ in (10b) which approximate $J_v(ka)$ and $H_v^{(2)}(ka)$ for $v \sim O(ka)$ reduce uniformly to the Debye asymptotic approximations when τ becomes large ($\tau = \frac{v - ka}{m}$) ; hence, in contrast to the approximation for $H^{(2)}_{v(\tau)}(k\rho)$ in (23), these Fock-type Airy functions remain valid as $v(\tau)$ becomes different from ka (i.e., for $|v - ka| > O(m)$) deep in the lit region. Instead of the approximation in (23), one could also approximate $H^{(2)}_{v(\tau)}(k\rho)$ for the near zone case by the Fock-type Airy function W_2 as follows, provided $k[\rho - a]<<ka$.

$$H^{(2)}_{v(\tau)}(k\rho) \approx \frac{i}{m\sqrt{\pi}} W_2\,(\tau - m^{-1}k[\rho - a]) \quad ; \quad k[\rho-a]<<ka. \tag{39}$$

But, employing the near zone approximation of Eq. (39) in I_2 of Eq. (10b) leads to integrals which are complicated functions of two parameters (namely, ψ and $[\rho - a]$); on the other hand, the result in (29) is in terms of simpler F and $\hat{P}_{\genfrac{}{}{0pt}{}{s}{h}}$ integrals which are each functions of only a single parameter.

A representation for U in the lit region which is interpretable in terms of the desired reflected ray geometry of Fig. 11 and which also is in terms of the F and $\hat{P}_{\substack{s\\h}}$ functions may be obtained in the following manner by incorporating an approximation for $H^{(2)}_{v(\tau)}(k\rho)$ which unlike (23) is valid even if v becomes quite different from ka in the lit region. One begins by introducing the Debye approximation for $H^{(2)}_{v(\tau)}(k\rho)$ which was previously indicated as

$$(40) \qquad H^{(2)}_{v(\tau)}(k\rho) \sim \sqrt{\frac{2}{\pi k\rho \sin\gamma}}\; e^{-ik\rho \sin\gamma + iv(\tau)\gamma + i\frac{\pi}{4}} \quad ;$$

$$v(\tau) = k\rho \cos\gamma \text{ and } v(\tau) < k\rho .$$

The condition that $v(\tau)<k\rho$ be satisfied in the lit zone is verified in the Appendix where the geometric optical reflected field result (corresponding to the second term on the R.H.S. of Eq. (37)) is developed in detail. Referring to this development in the Appendix, it is seen that in the lit region where $v<ka$, the following approximations are valid:

$$(41a) \qquad v(\tau) \approx v_o = ka \cos\tilde{\gamma}_o = k\rho \cos\gamma_o \qquad ; \quad \gamma \approx \gamma_o$$

$$(41b) \qquad \sin\tilde{\gamma}_o = \cos\theta^i, \text{ since } \tilde{\gamma}_o = \frac{\pi}{2} - \theta^i$$

$$(41c) \qquad \rho \sin\gamma \approx \rho \sin\gamma_o = \ell + a \sin\tilde{\gamma}_o = \ell + a\cos\theta^i$$

$$(41d) \qquad \psi \approx \gamma_o - 2\tilde{\gamma}_o$$

(Note: the geometrical signficances of (41) is shown in Fig. A-I in the Appendix.)

The quantity ψ has already be defined, and $\tilde{\gamma}_o$ is introduced in the Appendix. The subscript o in $v_o(\tau)$, γ_o and $\tilde{\gamma}_o$ refers to the geometrical optics reflected field saddle point condition which is also discussed in the Appendix. Incorporating $v(\tau)\gamma \approx v(\tau)\gamma_o$; $\rho \sin\gamma \approx \ell + a\cos\theta^i$ for the phase; and $\rho \sin\gamma \approx \ell$ for the far zone amplitude via (41a) and (41c) leads to the following far-zone approximation (in contrast to the near-zone approximation of Eq. (39)) for $H^{(2)}_{v(\tau)}(k\rho)$ in the lit zone.

$$(42) \qquad H^{(2)}_{v(\tau)}(k\rho) \sim \sqrt{\frac{2}{\pi\, k\, \ell}}\; e^{-ik(\ell + a\cos\theta^{i}) + iv(\tau)\gamma_0 + i\frac{\pi}{4}} \,.$$

Next, incorporating (41d), (42), and $\tilde{Q}\, W_1(\tau) = \tilde{Q}\, W_2(\tau) + 2\, i\tilde{Q}\, V(\tau)$ into (10b) yields:

$$(43) \qquad I_2 \sim -\sqrt{\frac{2}{k\ell}}\; e^{-ik\ell\, - ika\cos\theta^{i}}\; m\, e^{-ika(-2\,\tilde{\gamma}_0)}$$

$$\cdot \left[\frac{e^{-i\frac{\pi}{4}}}{2\sqrt{\pi}\,[m(-2\,\tilde{\gamma}_0)]} + \frac{e^{-i\frac{\pi}{4}}}{\sqrt{\pi}} \int_{-\infty}^{\infty} \frac{\tilde{Q}\, V(\tau)}{\tilde{Q}\, W_2(\tau)}\, e^{-im(-2\,\tilde{\gamma}_0)\tau}\, d\tau \right] .$$

One now defines ξ' for the lit region as

$$(44) \qquad \xi' \equiv -\,2\, m \sin\tilde{\gamma}_0 = -\,2\, m\cos\theta^{i} \quad ; \quad \xi' < 0 \text{ in the lit region.}$$

Thus, the exponential terms involving $\tilde{\gamma}_0$ in (43) may be written as

$$(45a) \qquad e^{-ika(-2\,\tilde{\gamma}_0)} \approx e^{2\, ika\cos\theta^{i} \,-\, i(\xi')^3/12}$$

and

$$(45b) \qquad e^{-im(-2\,\tilde{\gamma}_0)\tau} \approx e^{-i\xi'\tau}$$

provided that ξ' is sufficiently small in comparison with m which is assumed large so that terms $O\left(\frac{1}{[2m]^2}\right)$ and higher may be neglected in the exponent. This approximation is valid in the transition region. One notes that the approximation in (45a) and (45b) follow directly from the expansion

$$(45c) \qquad -\tilde{\gamma}_o = \sin^{-1}\frac{\xi'}{2m} = \frac{1}{2m}\xi' + \frac{1}{6(2m)^3}(\xi')^3 + \frac{3}{40(2m)^5}(\xi')^5 + \cdots ,$$

$$\text{with} \left(\frac{\xi'}{2m}\right)^2 < 1.$$

Employing (45a) and (45b) into (43) yields

$$(46) \qquad I_2 \sim -\sqrt{\frac{2}{k\ell}}\, e^{-ik\ell\, -ika\cos\theta^i}\, m\, e^{i2ka\cos\theta^i} \cdot$$

$$\cdot\, e^{-i(\xi')^3/12}\left[\frac{e^{-i\frac{\pi}{4}}}{2\sqrt{\pi}\xi'} + \hat{P}_{\substack{s\\h}}(\xi')\right] ,$$

which is valid in the far zone. In the lit region far from SB_1, $\xi' << 0$, and $\hat{P}_{\substack{s\\h}}(\xi)$ may be replaced by (35) to yield

$$(47) \qquad I_2 \sim \mp\, e^{ika\cos\theta^i}\sqrt{\frac{\rho_r}{\ell}}\, e^{-ik\ell} ,$$

which does indeed agree with the far zone geometrical optics reflected field. The term $e^{ika\cos\theta^i}$ corresponds exactly to $U^i(Q_r)$, and $\{\mp\}$ denotes the reflection coefficient values as in (37). It is now evident that one can employ ray optics to generalize (46) so that it yields the near zone geometrical optics reflected field as in (37). According to ray optics, the far zone energy spread factor $\sqrt{\frac{\rho_r}{\ell}}$ in (47) must be simply replaced by its corresponding near zone factor $\sqrt{\frac{\rho_r}{\rho_r + \ell}}$ (as in (37)) for the reflected ray tube in order to extend (47) to the near zone case; the latter is tantamount to replacing $\frac{1}{\sqrt{\ell}}$ in (46) with $\frac{1}{\sqrt{\rho_r + \ell}}$ thereby generalizing (46) to the near zone case.

To be consistent, it is also necessary to modify the result for I_1 of (10a) for the lit region in the same manner as done above for I_2 of (10b). Without giving all the details (since these involve essentially the same physical arguments as in the treatment of I_2), the result for I_1 in the lit region becomes

(48a) $$I_1 \sim e^{ik\rho\cos\phi} H(-\theta) - e^{ika\cos\theta^i} \cdot \left\{ \frac{m\, e^{-i\frac{\pi}{4}}}{\sqrt{2\pi k}\,\xi'} \left(- F[kL' \frac{\xi'^2}{2m^2}] \right) \right\} e^{-\frac{i(\xi')^3}{12}} \frac{e^{-ik\ell}}{\sqrt{\ell + \rho_r}} ,$$

with

(48b) $$L' \doteq \ell , \text{ for } \xi'<0 .$$

Finally, combining (46) (together with it's near zone modification) and (48), one obtains the required result for U in the lit region; namely,

(49) $$U(P_L) \sim U^i(P_L) + U^i(Q_R) \left[\frac{-m\, e^{-i\frac{\pi}{4}}}{\sqrt{2\pi k}\,\xi'} e^{-\frac{i(\xi')^3}{12}} \cdot \left\{ 1 - F[kL' \frac{\xi'^2}{2m^2}] \right\} \right] \frac{e^{-ik\ell}}{\sqrt{\ell + \rho_r}} + U^i(Q_R) \left[- m \sqrt{\frac{2}{k}}\, e^{-\frac{i(\xi')^3}{12}} \hat{P}_{\substack{s\\h}}(\xi') \right] \frac{e^{-ik\ell}}{\sqrt{\ell + \rho_r}} \quad ; \quad \xi'<0.$$

It is easily verified that far from SB_1 ($\xi'<<0$), $F[kL' \frac{\xi'^2}{2m^2}] \to 1$ and $\hat{P}_{\substack{s\\h}}(\xi')$ behaves as in (35) so that in the deep lit regions Eq. (49) reduces exactly to the geometrical optics result of Eq. (37). Furthermore, Eq. (49) is also valid for $\theta^i \to \pi/2$ (i.e., near SB_1) since it agrees in this limiting case with the expression in (29) for $\xi<0$. In addition, Eq. (49) reduces to Eq. (31), thereby assuring the boundedness and continuity of the field across SB_1. Thus, the result for U in (49) for the lit region reduces to the geometrical optics field deep in the illuminated region where the latter is indeed valid, and at the same time it has the proper behavior required to ensure the continuity of the field across SB_1.

III. NUMERICAL RESULTS

In this section, numerical results are presented for the near zone total field surrounding a perfectly-conducting circular cylinder excited by a plane wave. The GTD method is employed to describe the field exterior to the cylinder in terms of the geometrical optics incident and reflected rays for the lit region, and in terms of the surface diffracted rays for the shadow region, respectively; these results for the TE_z (hard boundary) case are indicated in Figs. 12(a) - 20(a) for different size cylinders and near field distances. It is seen that the GTD solution shown by a dashed line becomes discontinuous at the shadow boundaries. On the other hand, the present transition region solution (based on (27) for the shadow, and on (49) for the lit region) as indicated by a solid line is continuous across the shadow boundaries, and it blends smoothly into the GTD solution outside the transition region. These GTD and transition region solutions corresponding to Figs. 12(a) - 20(a) are combined into a single, composite GTD-transition solution which is shown by a smooth solid curve in Figs. 12(b) - 20(b), respectively. The composite GTD-transition results are compared against results which are based on an exact eigenfunction series solution for these cases; the eigenfunction results are shown by dots in Figs. 12(b) - 20(b) for these cases. Figures 12(b) - 20(b) indicate that the comparison between the numerical results obtained from the exact eigenfunction solution, and the composite GTD-transition solution is very good, thereby confirming the accuracy of the uniform result for the transition region presented in section II. Additional comparisons of the composite GTD-transition solutions with the corresponding eigenfunction solutions are indicated in Figs. 21-22 for the TM_z (soft boundary) case, respectively; again the agreement is very good for these cases. It is seen that the accuracy of the transition region solution for very small ka and kρ is as good as the accuracy of the geometrical optics result.* As ka and kρ increase, our asymptotic transition field solution becomes increasingly accurate as do the GTD (surface diffracted and geometric optical) ray fields which also are asymptotic approximations. For calculating the GTD field in the shadow region, the inclusion of only two surface ray modes are found to be sufficiently accurate (see (33)). Unfortunately, there appears to be a small error in the p* function plotted in Fig. 8(a); this error is noticeable for ranges of ξ which occur for small kρ and ka in the TM_z case. Presently, improved curves for the amplitude and phase of $p^*(\xi)$ are being obtained.

---

*In the GTD calculation for the lit region (or the geometrical optics region), the surface rays that have crept around the opposite side of the cylinder have been neglected; but the field of these rays is included with the transition field in the calculation shown by the solid line.

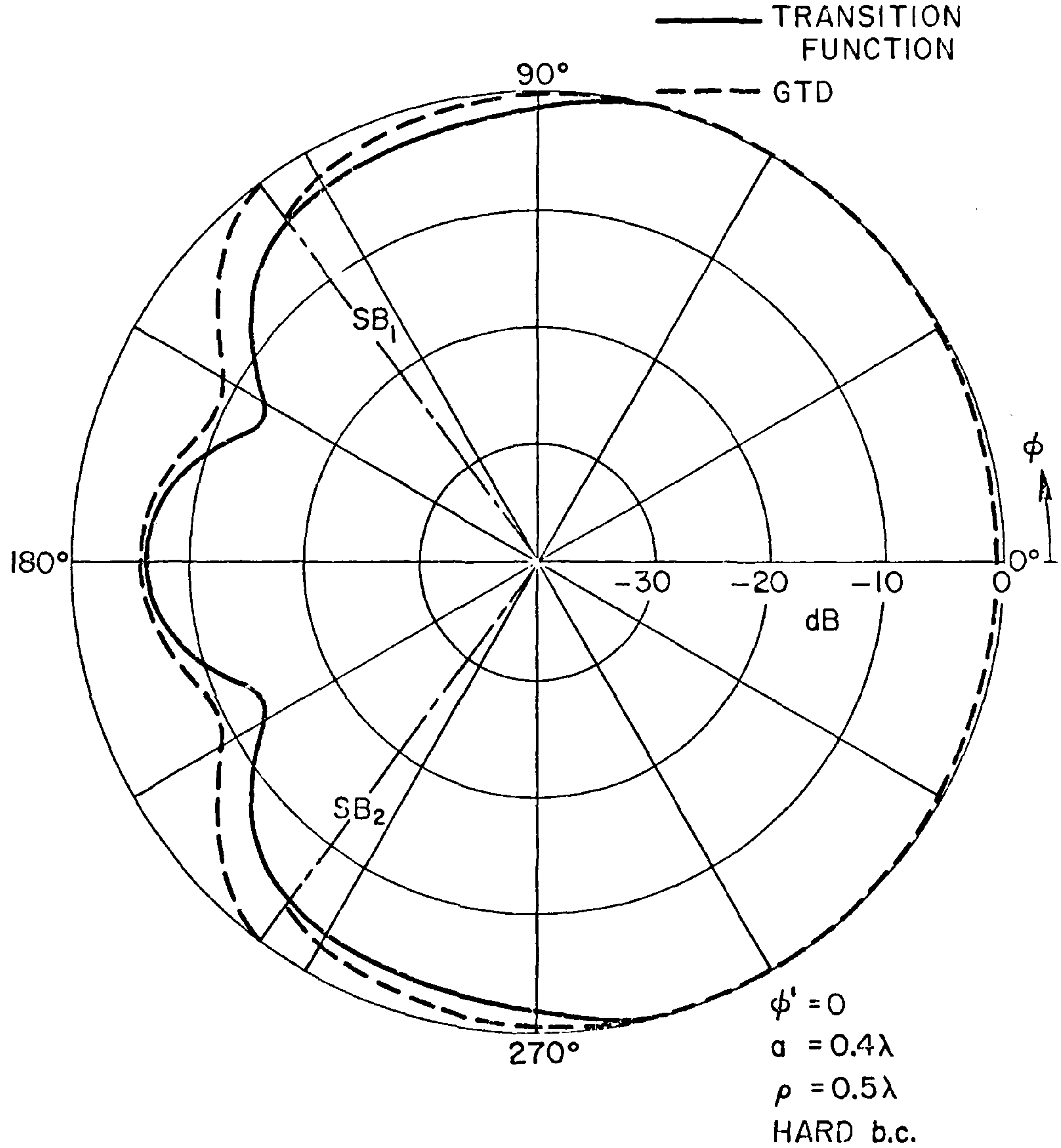

Fig. 12(a). Field surrounding a circular cylinder illuminated by a TE_z plane wave. Calculations based on GTD and the transition solution.

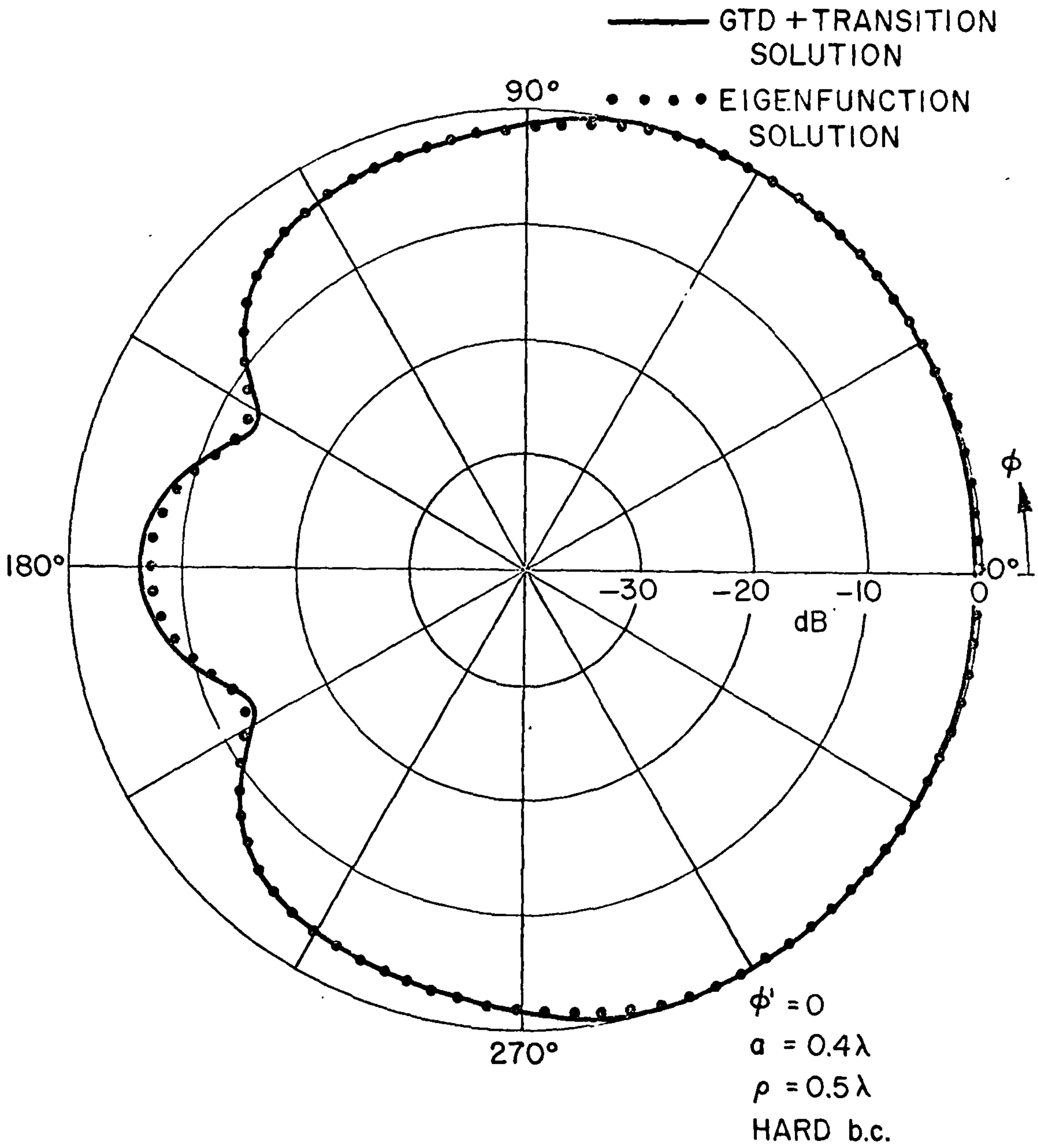

Fig. 12(b). Comparison of the composite GTD plus transition solution of Fig. 12(a) with the exact solution.

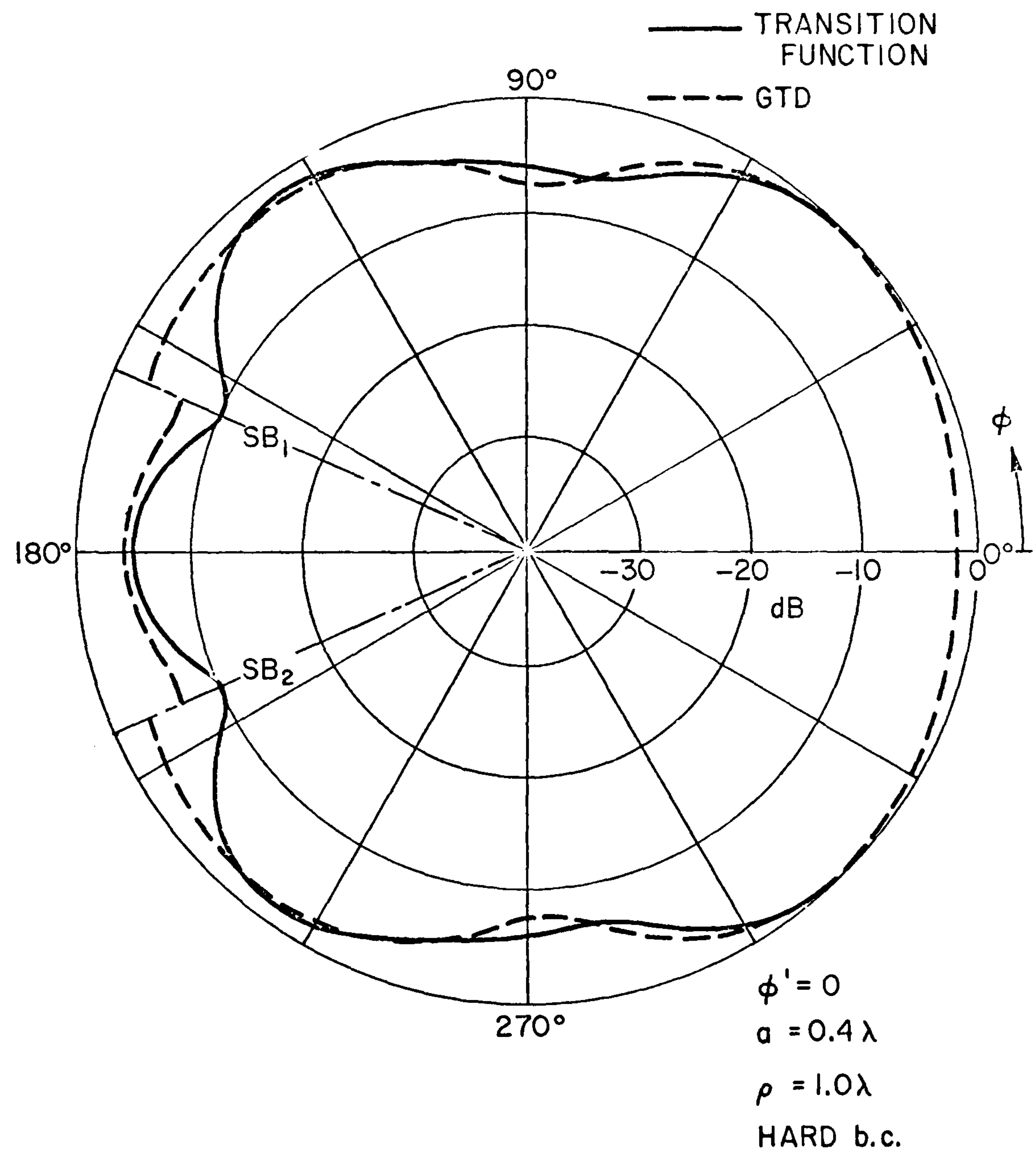

Fig. 13(a). Field surrounding a circular cylinder illuminated by a TE_z plane wave. Calculations based on GTD and the transition solution.

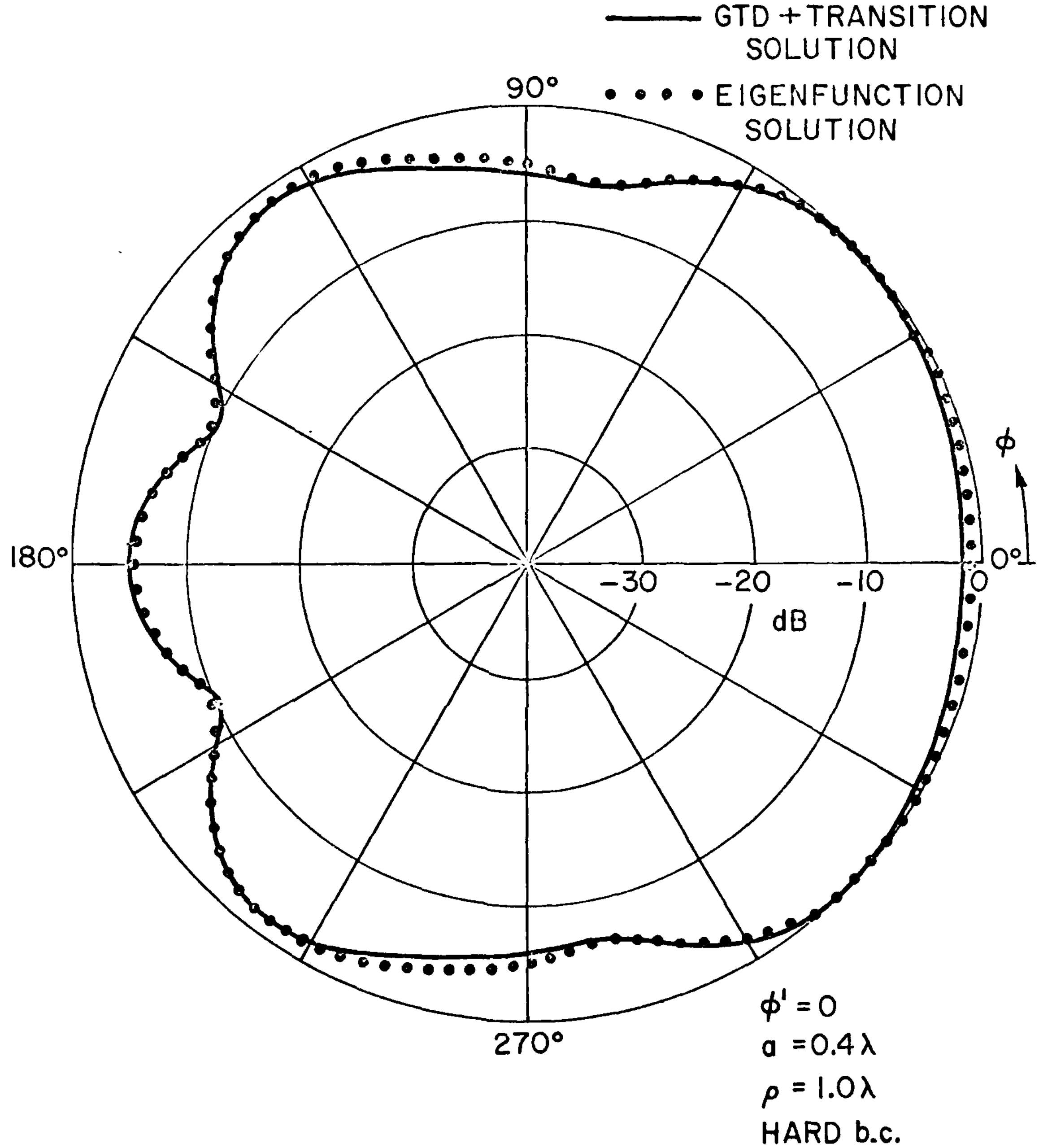

Fig. 13(b). Comparison of the composite GTD plus transition solution of Fig. 13(a) with the exact solution.

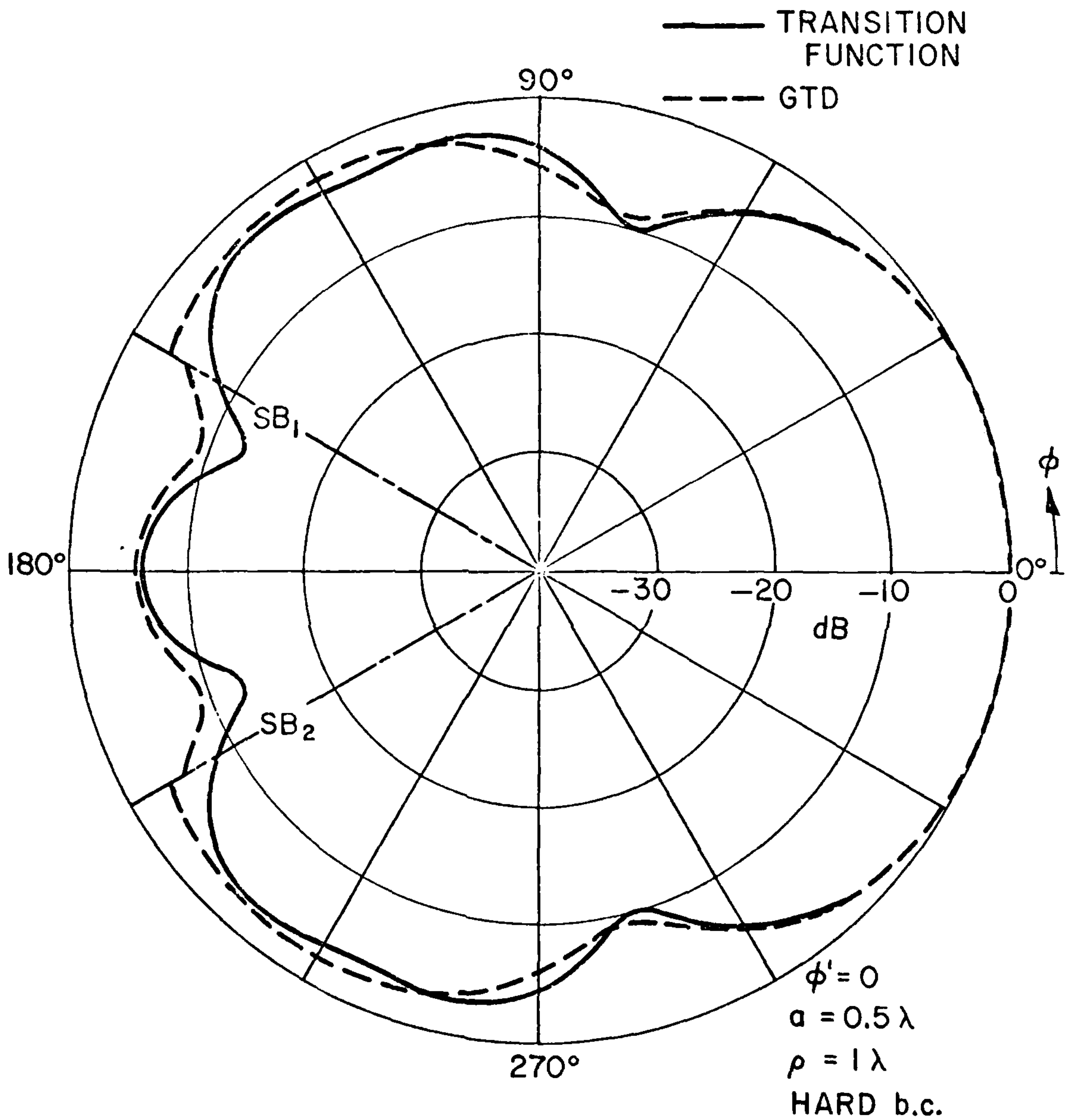

Fig. 14(a). Field surrounding a circular cylinder illuminated by a TE_z plane wave. Calculations based on GTD and the transition solution.

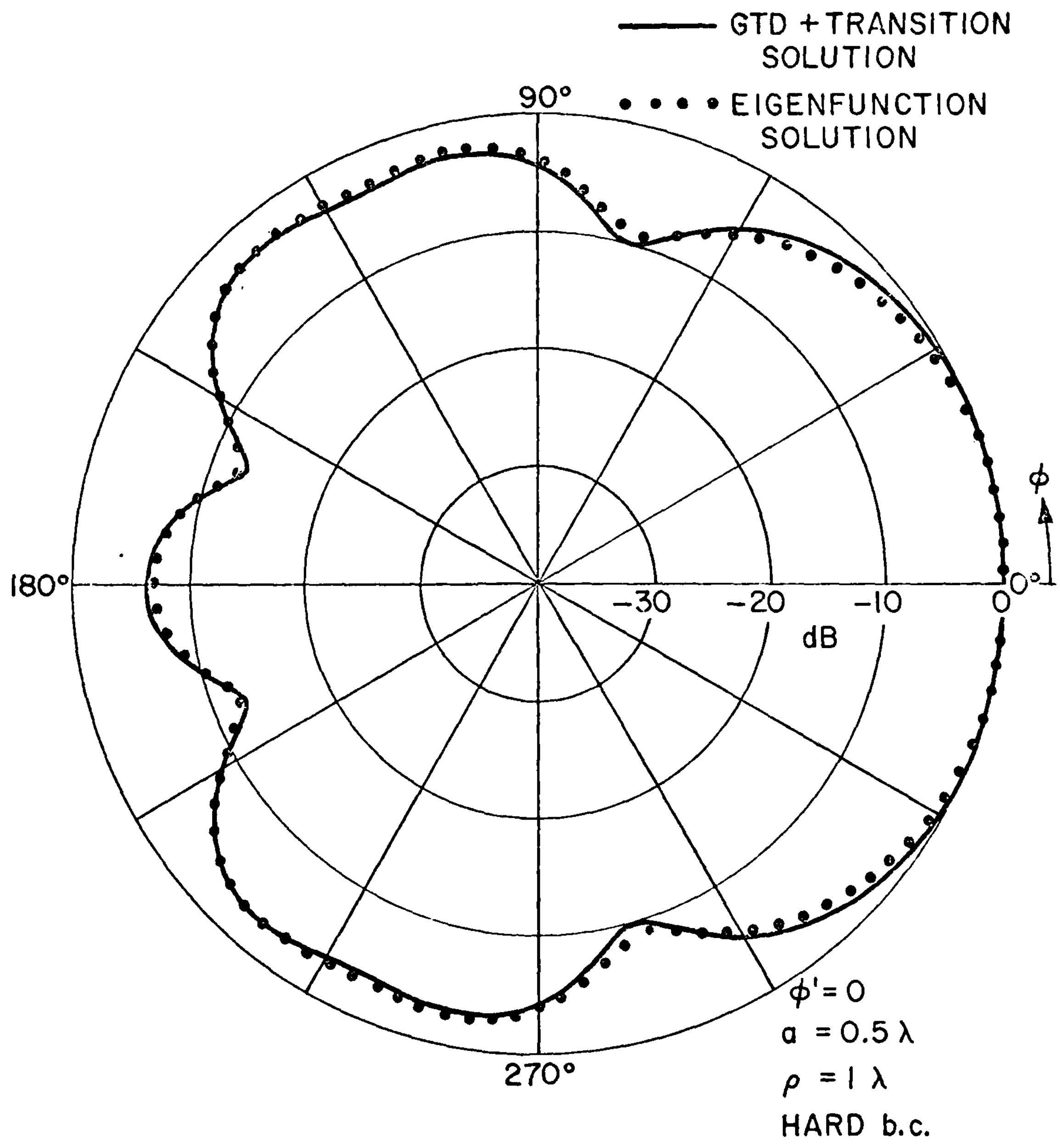

Fig. 14(b). Comparison of the composite GTD plus transition solution of Fig. 14(a) with the exact solution.

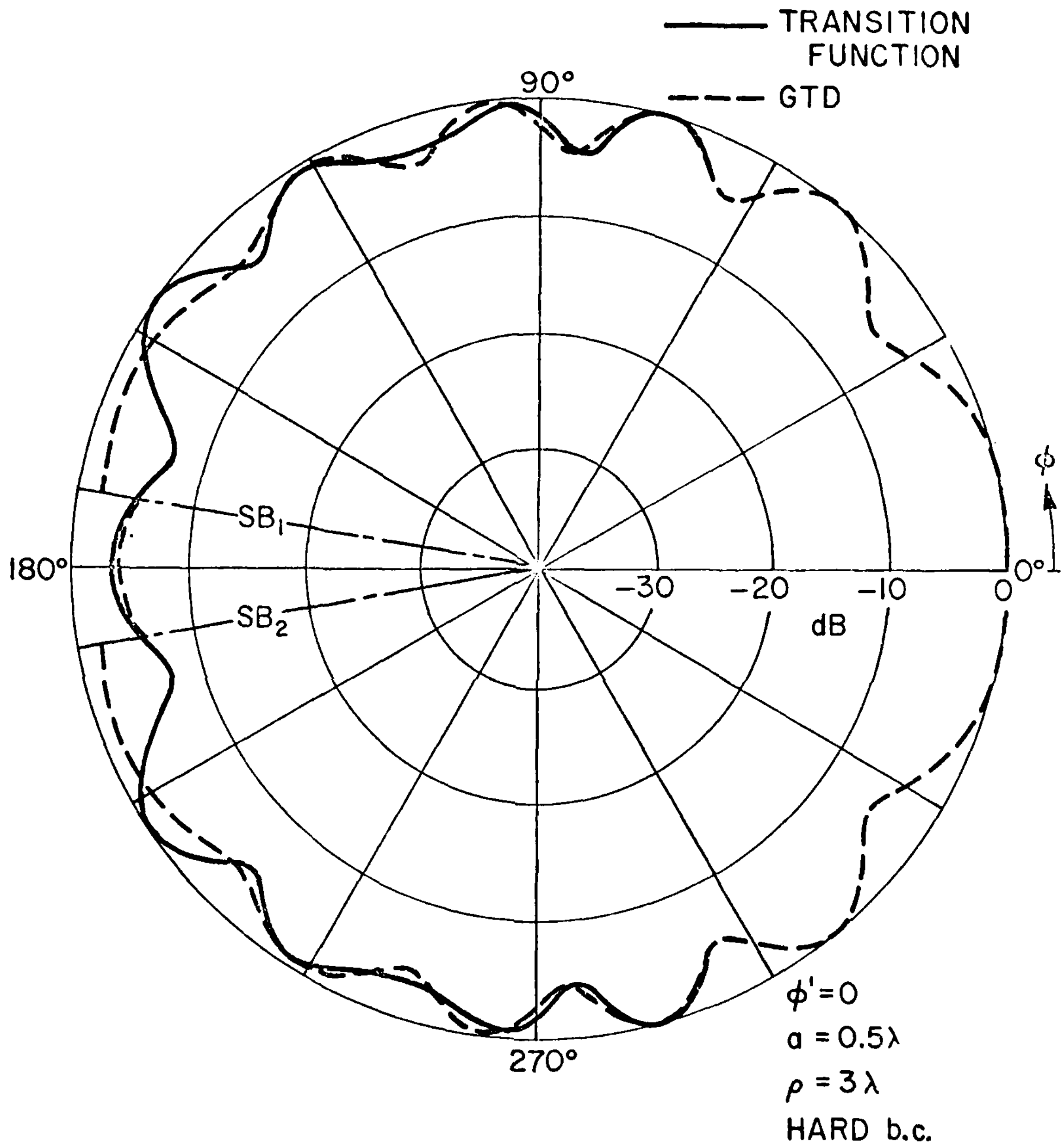

Fig. 15(a). Field surrounding a circular cylinder illuminated by a TE_z plane wave. Calculations based on GTD and the transition solution.

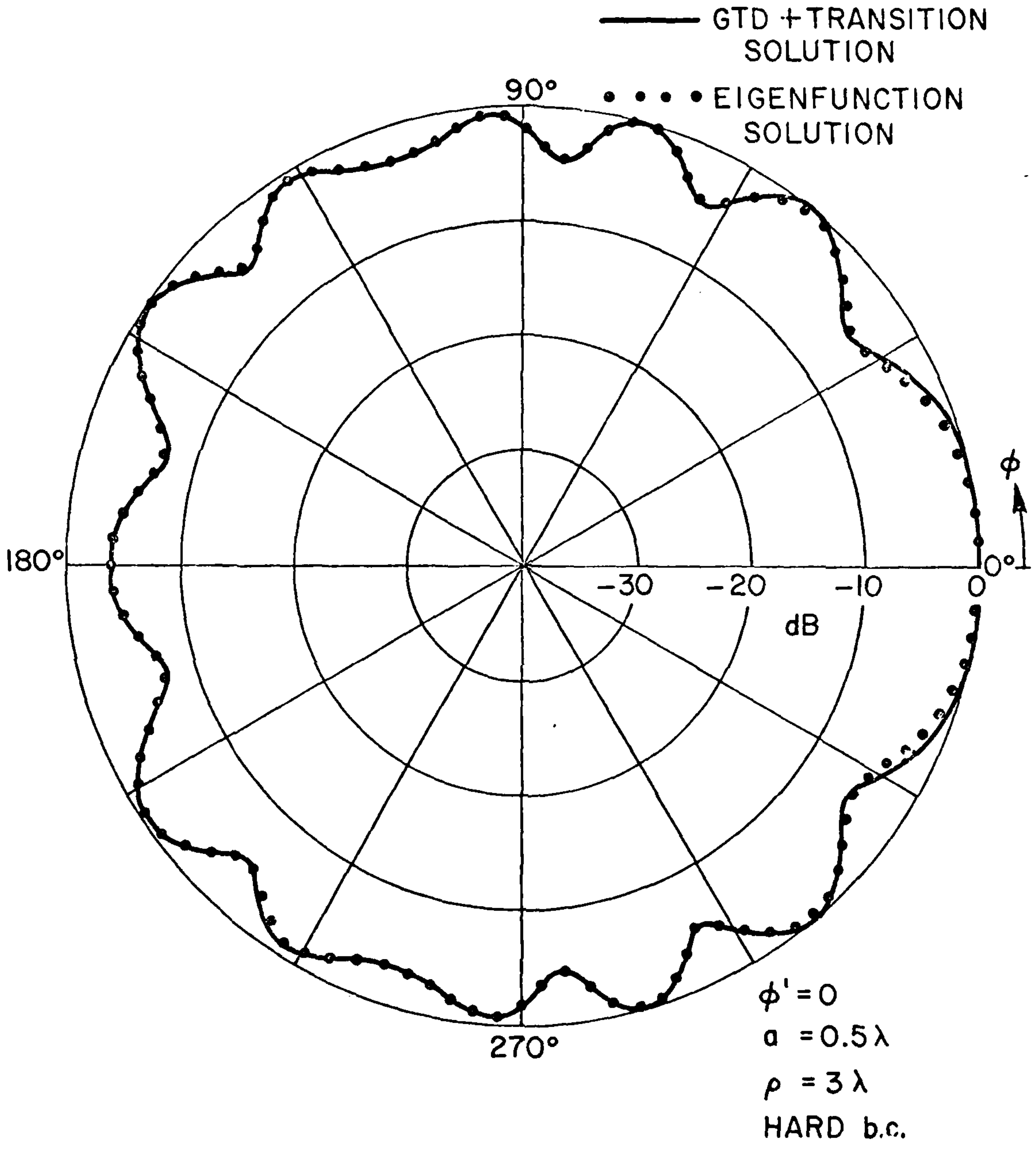

Fig. 15(b). Comparison of the composite GTD plus transition solution of Fig. 15(a) with the exact solution.

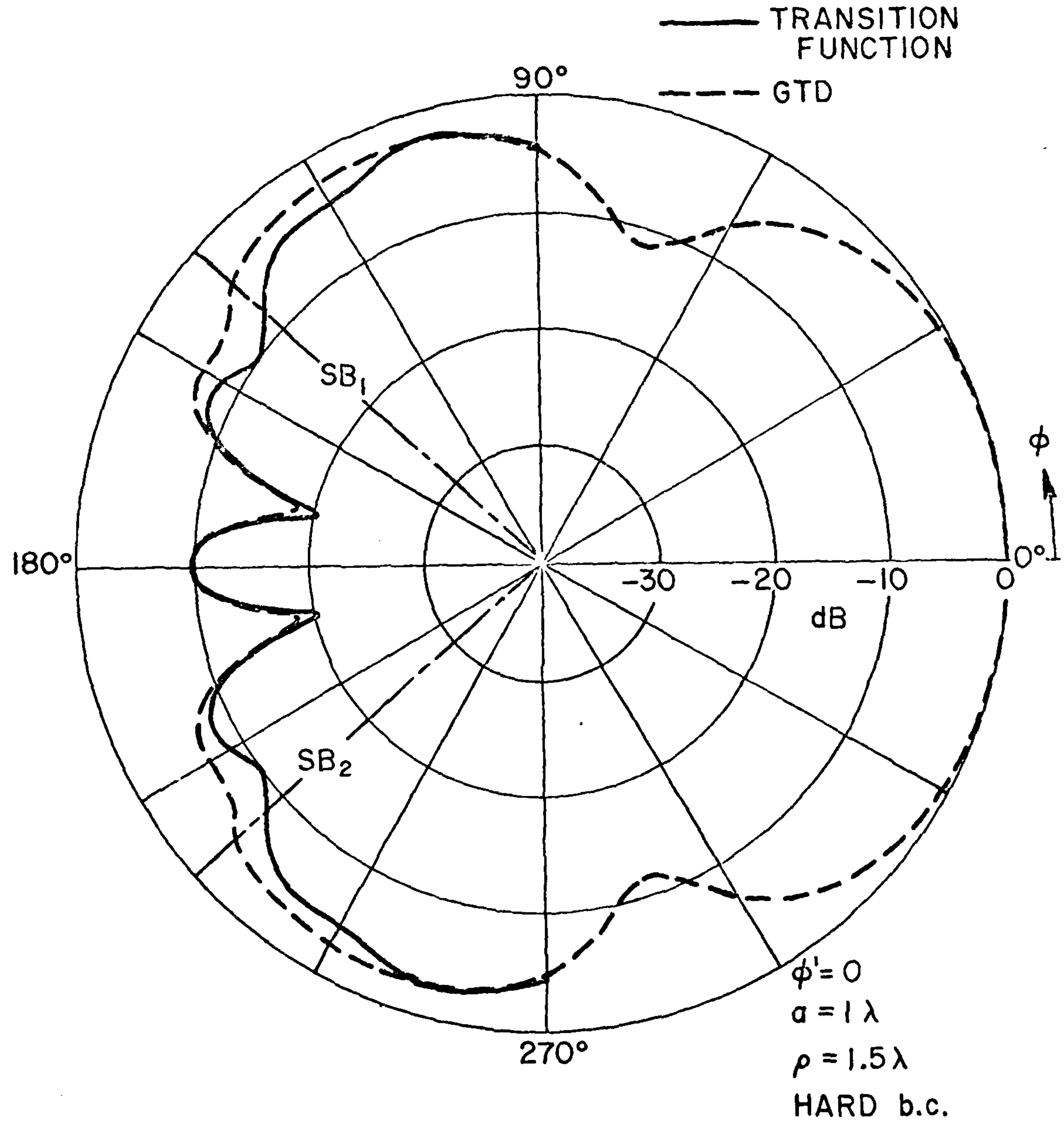

Fig. 16(a). Field surrounding a circular cylinder illuminated by a TE_z plane wave. Calculations based on GTD and the transition solution.

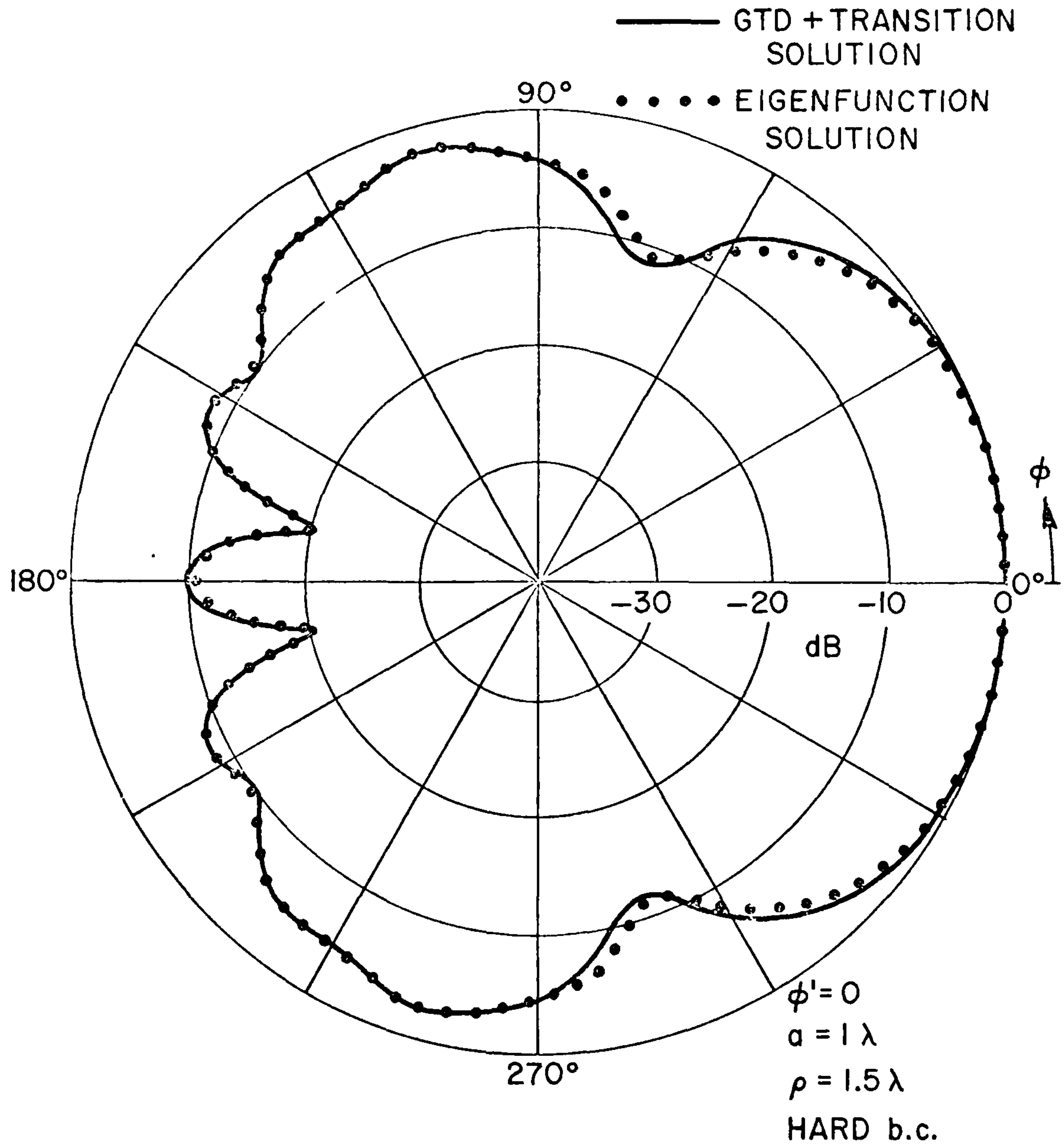

Fig. 16(b). Comparison of the composite GTD plus transition solution of Fig. 16(a) with the exact solution.

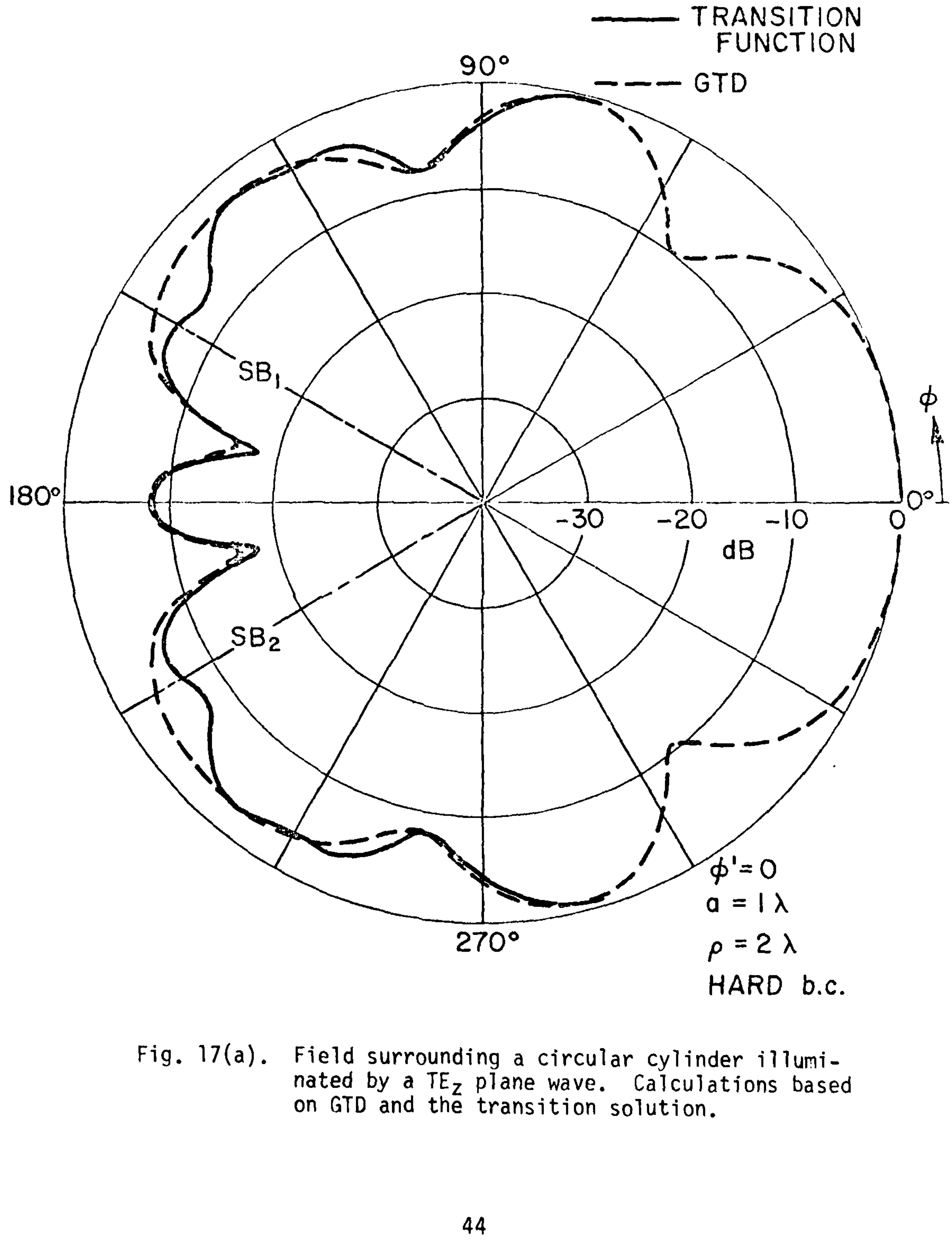

Fig. 17(a). Field surrounding a circular cylinder illuminated by a TE_z plane wave. Calculations based on GTD and the transition solution.

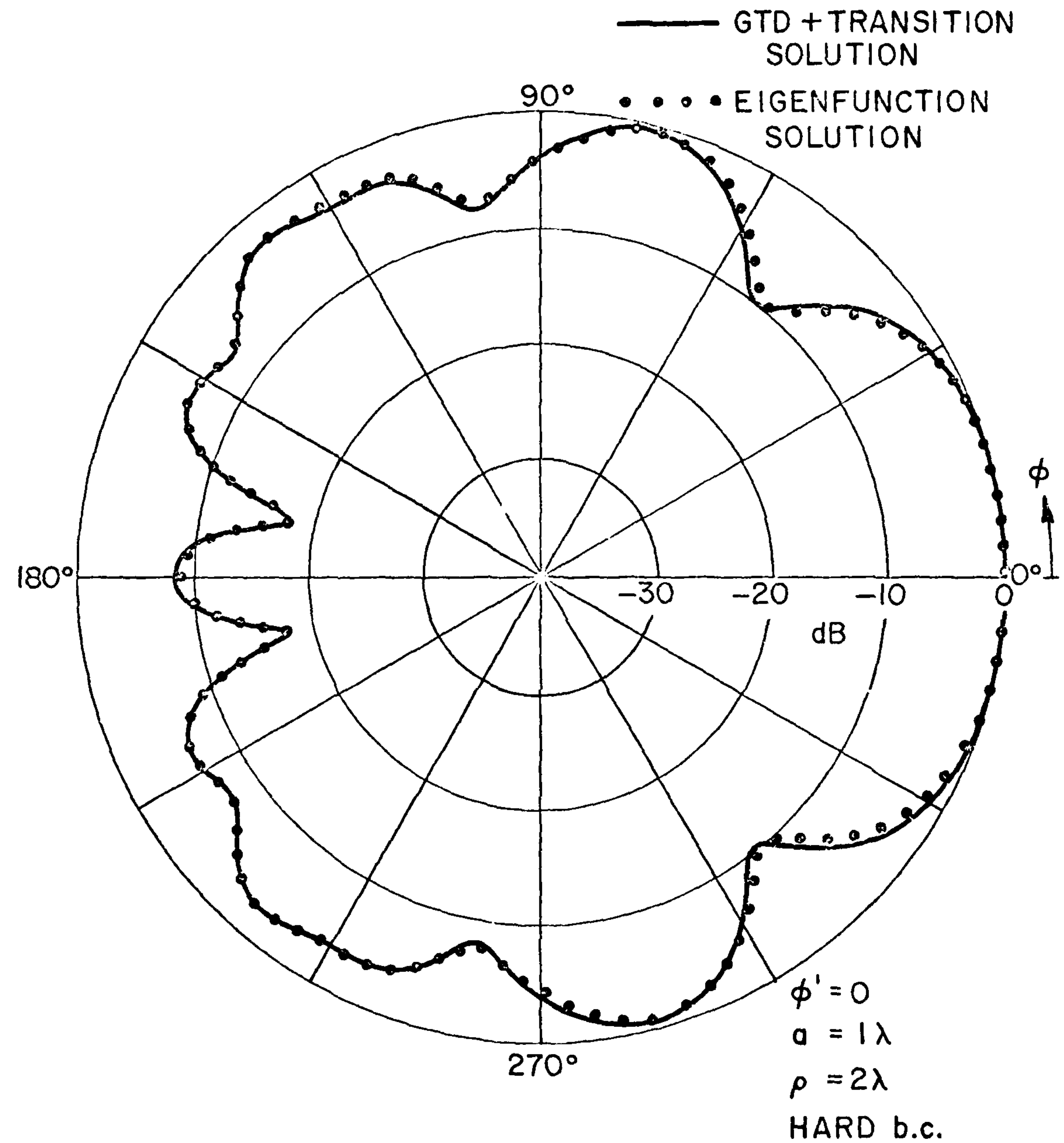

Fig. 17(b). Comparison of ... composite GTD plus transition solution of Fig. 17(a) with the exact solution.

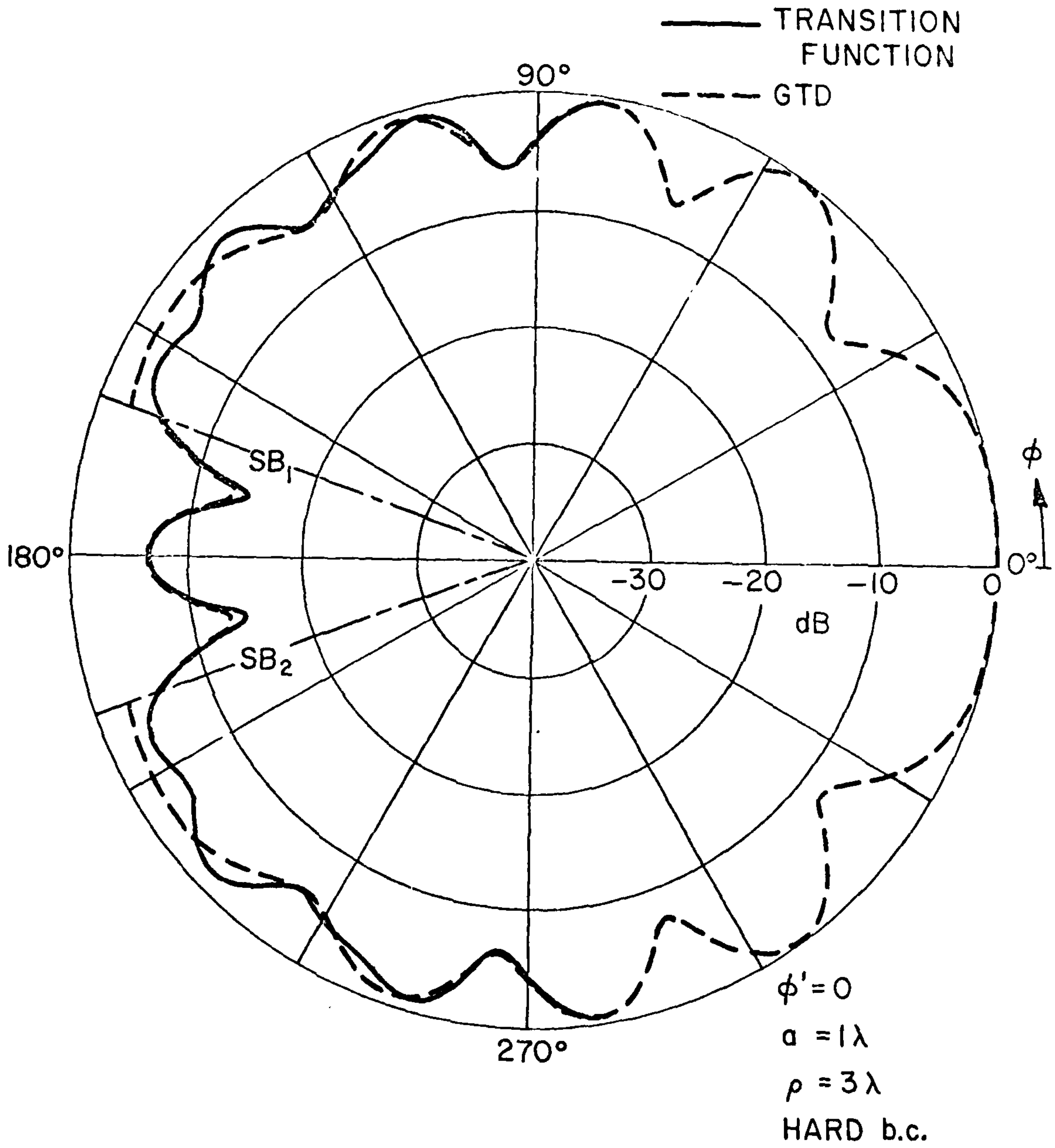

Fig. 18(a). Field surrounding a circular cylinder illuminated by a TE_z plane wave. Calculations based on GTD and the transition solution.

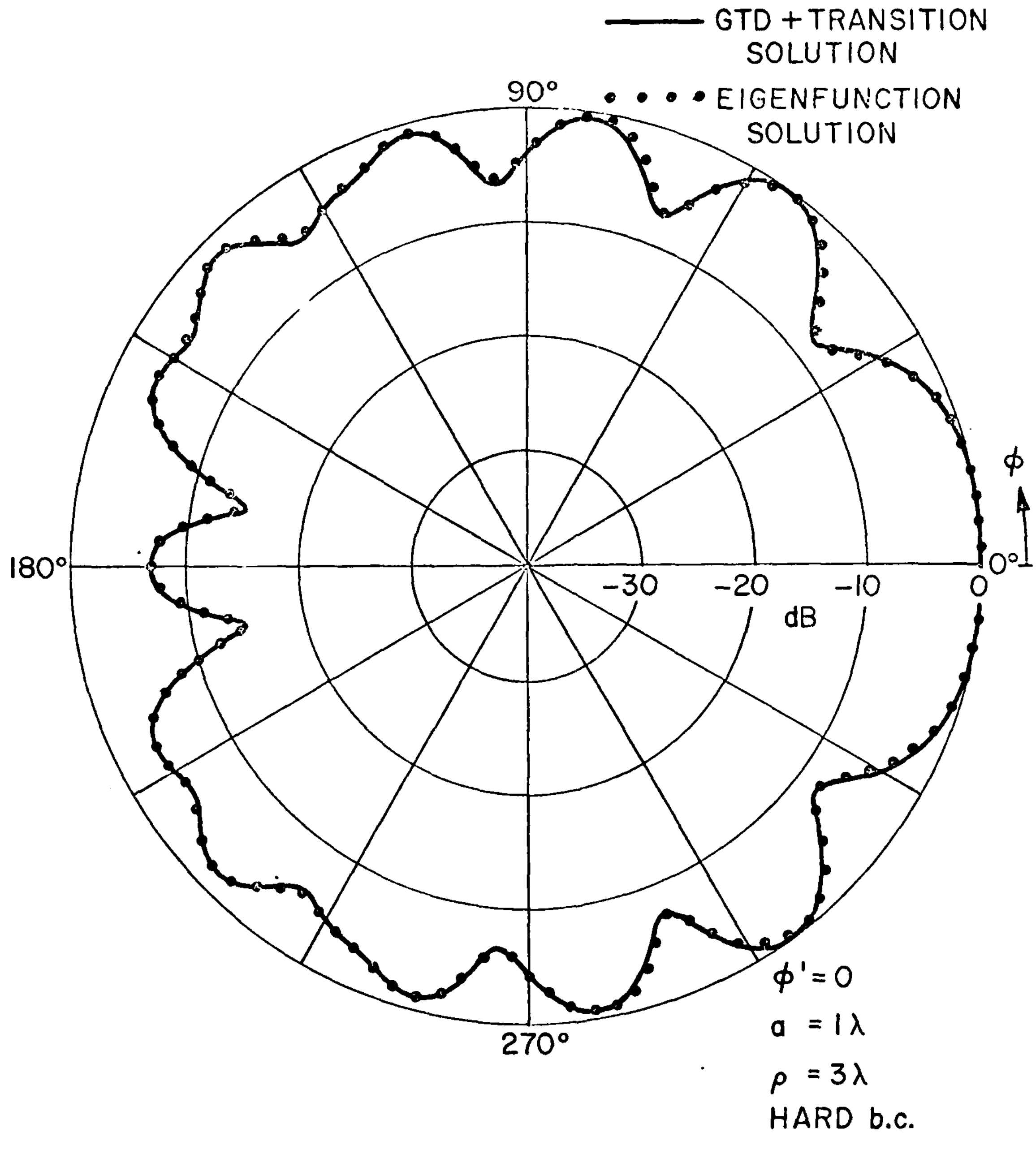

Fig. 18(b). Comparison of the composite GTD plus transition solution of Fig. 18(a) with the exact solution.

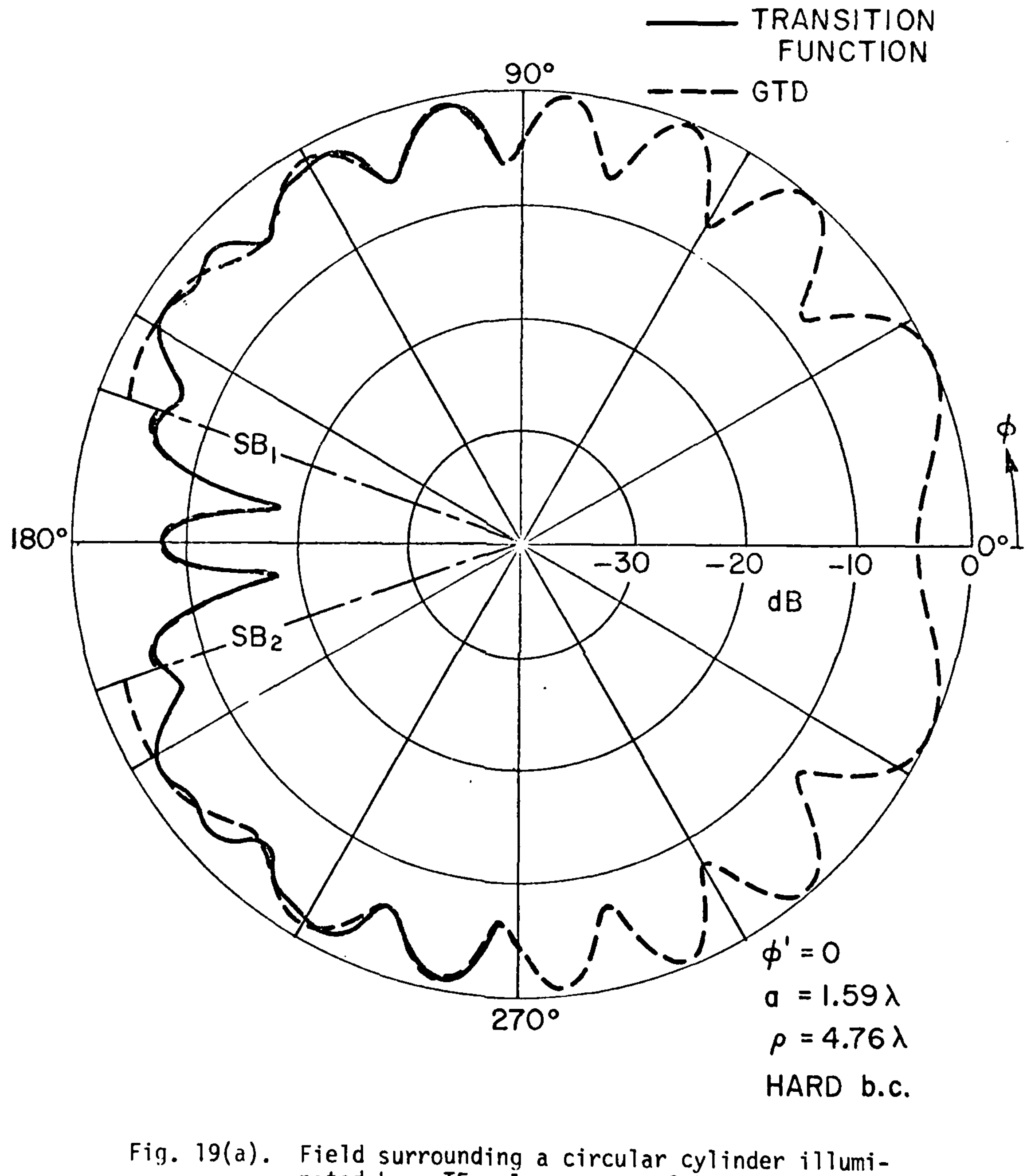

Fig. 19(a). Field surrounding a circular cylinder illuminated by a TE_z plane wave. Calculations based on GTD and the transition solution.

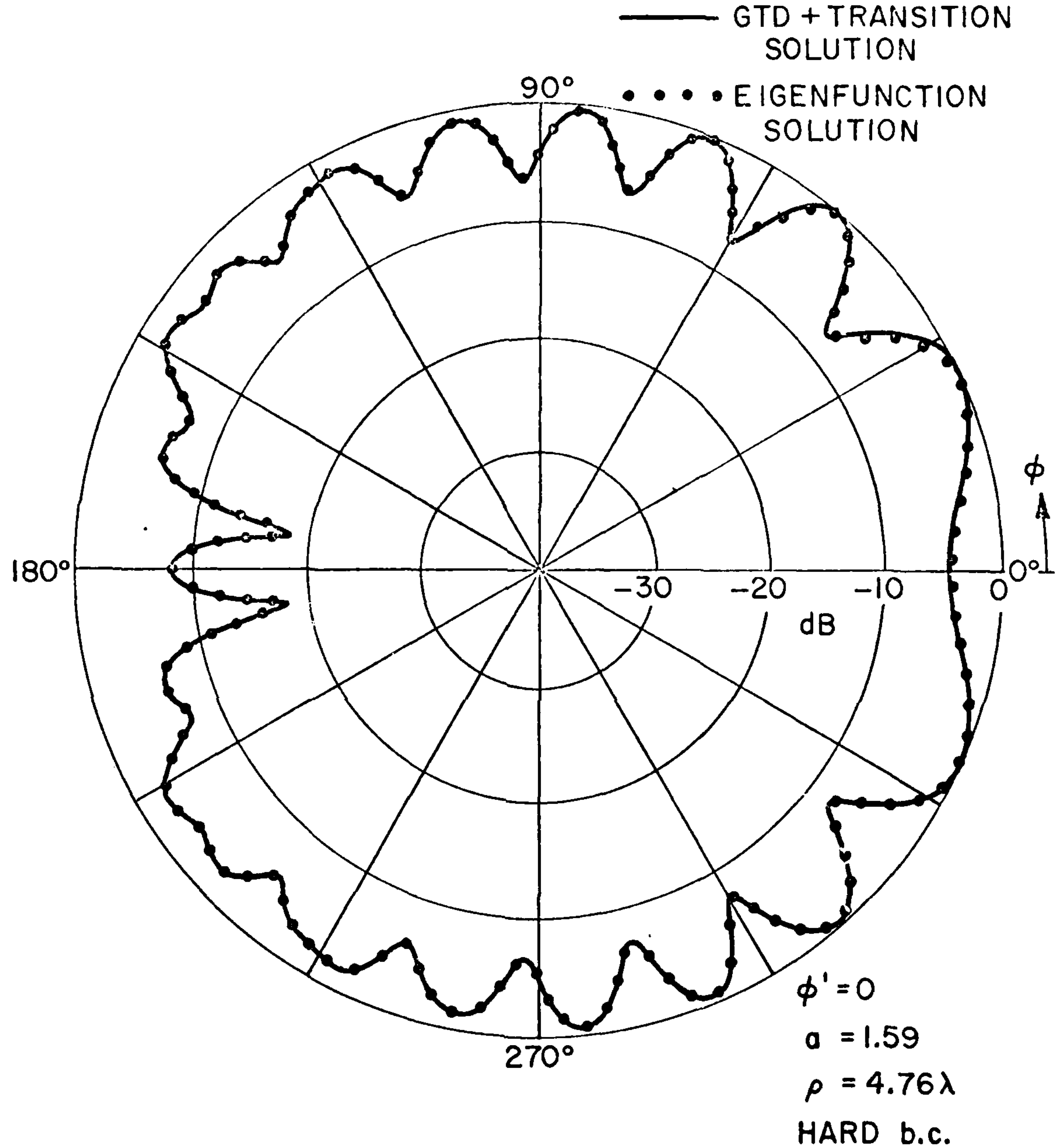

Fig. 19(b). Comparison of the composite GTD plus transition solution of Fig. 19(a) with the exact solution.

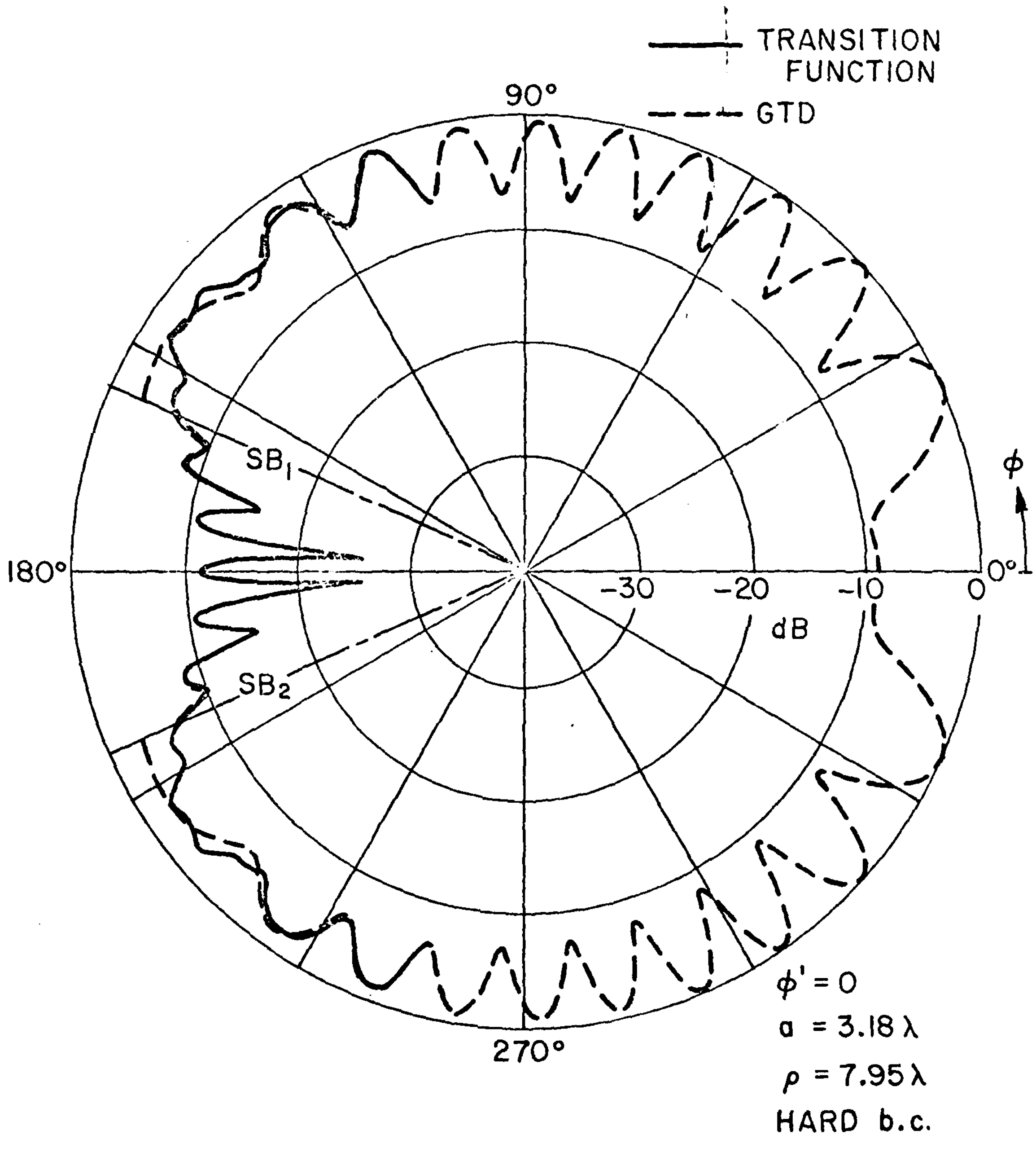

Fig. 20(a). Field surrounding a circular cylinder illuminated by a TE_z plane wave. Calculations based on GTD and the transition solution.

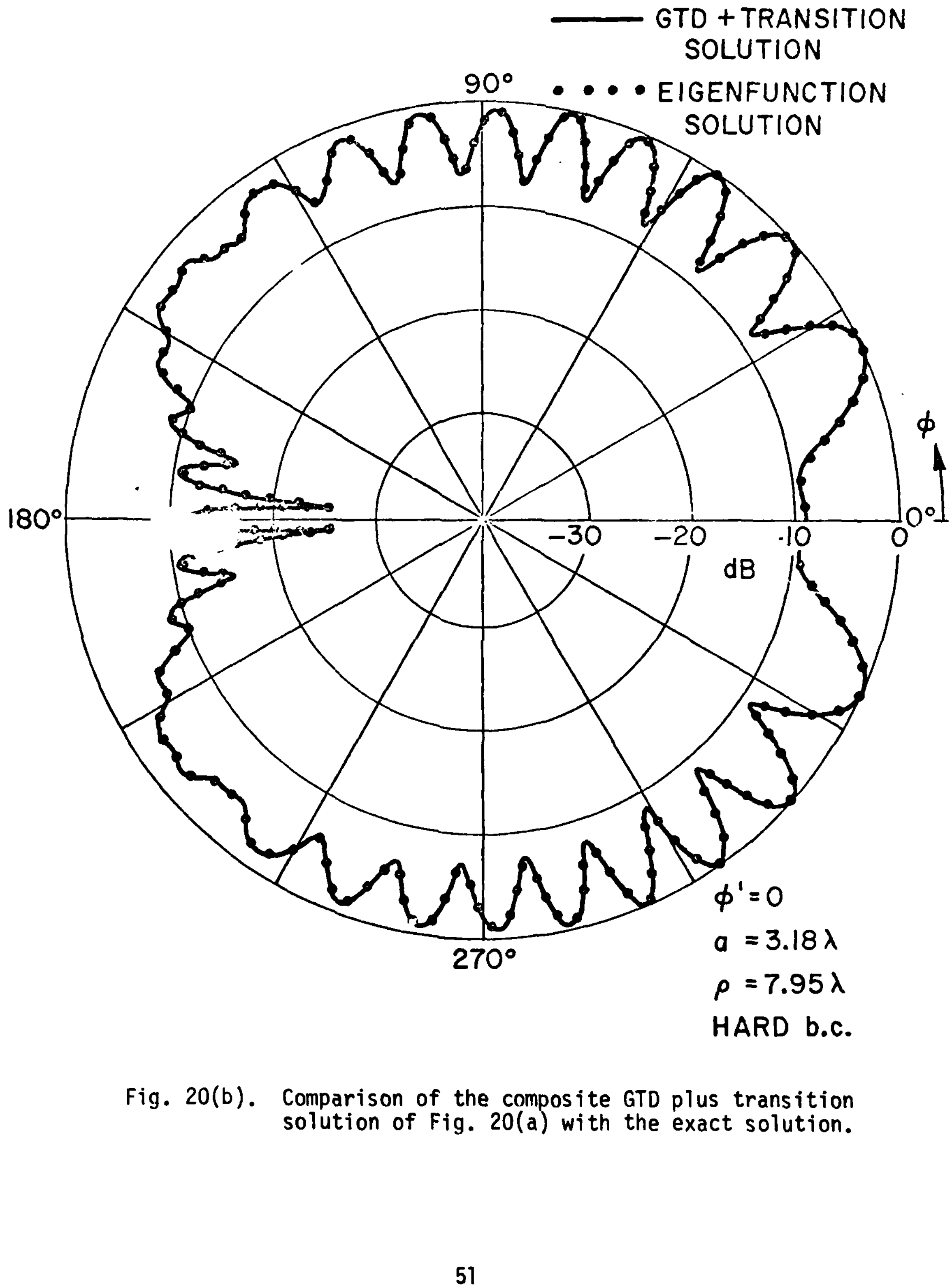

Fig. 20(b). Comparison of the composite GTD plus transition solution of Fig. 20(a) with the exact solution.

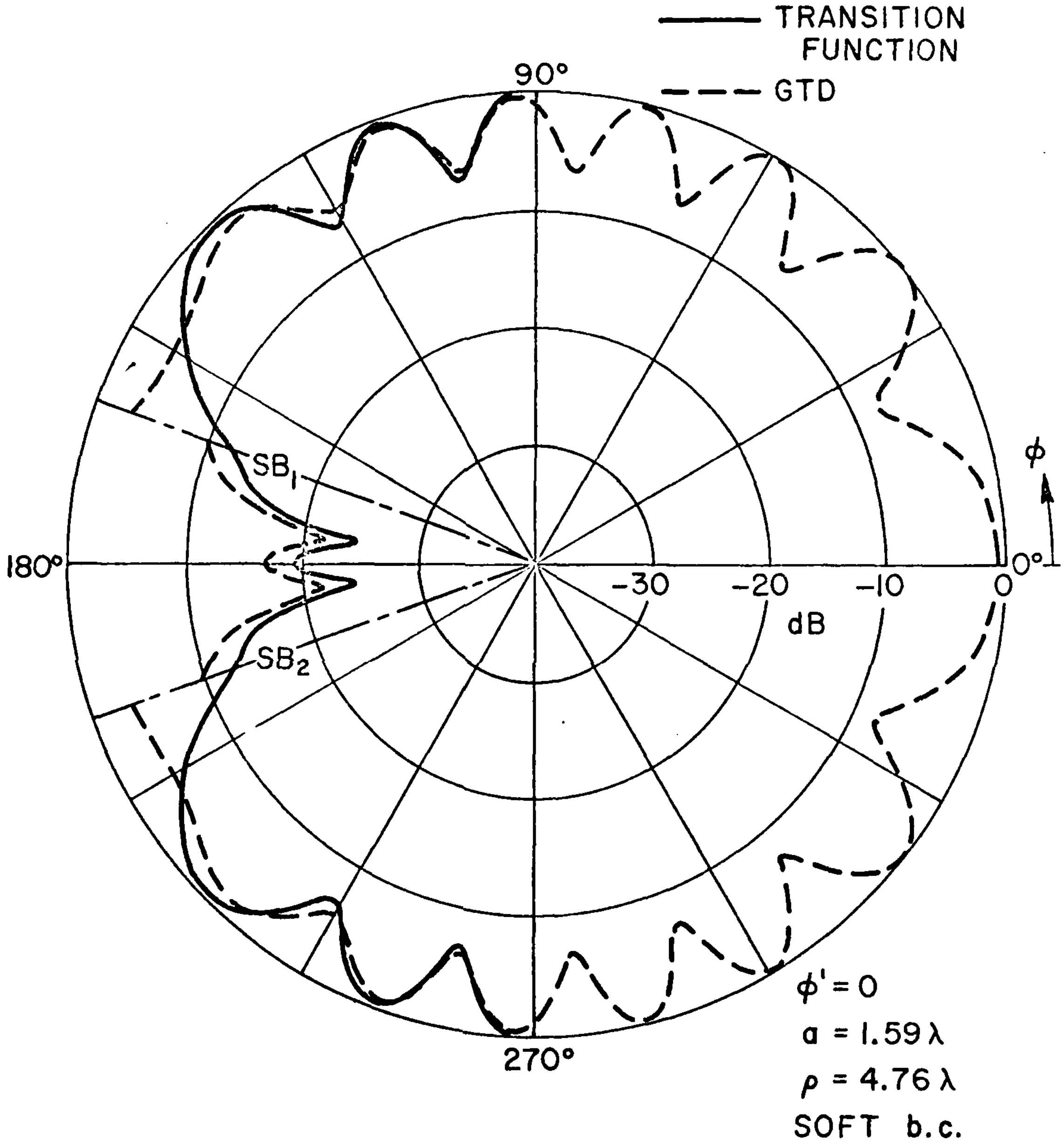

Fig. 21(a). Field surrounding a circular cylinder illuminated by a TM_z plane wave. Calculations based on GTD and the transition solution.

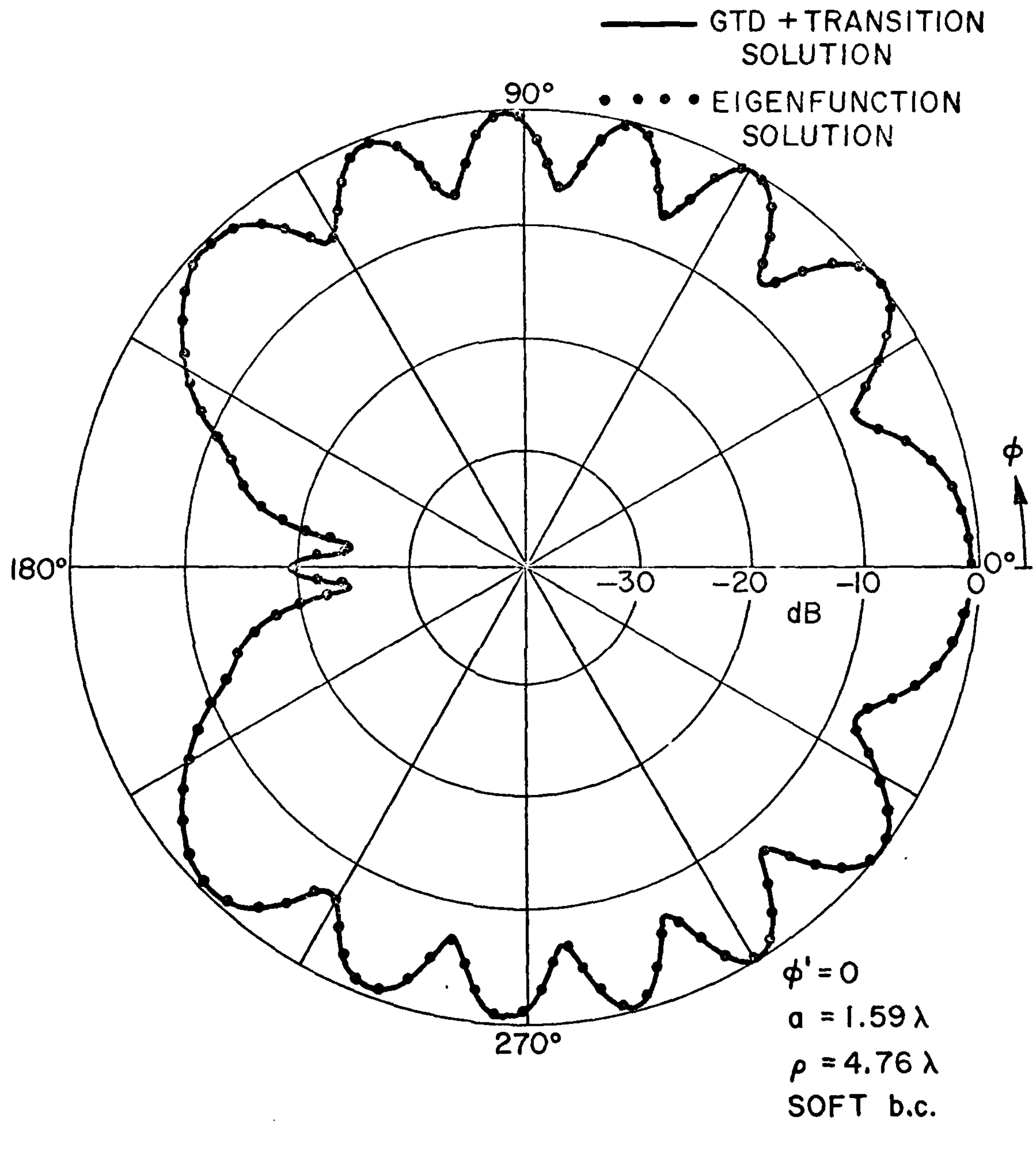

Fig. 21(b). Comparison of the composite GTD plus transition solution of Fig. 21(a) with the exact solution.

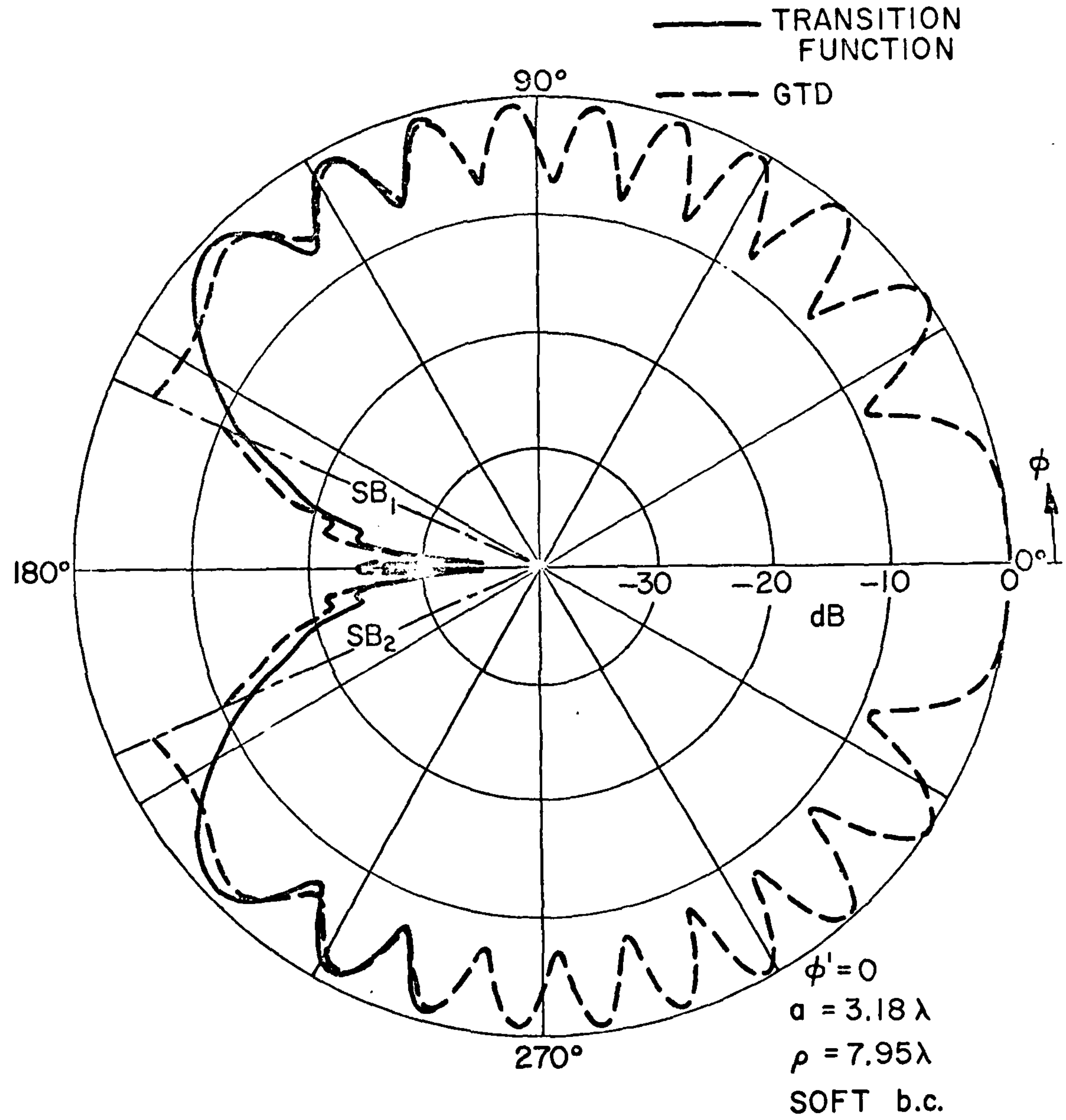

Fig. 22(a). Field surrounding a circular cylinder illuminated by a TM_z plane wave. Calculations based on GTD and the transition solution.

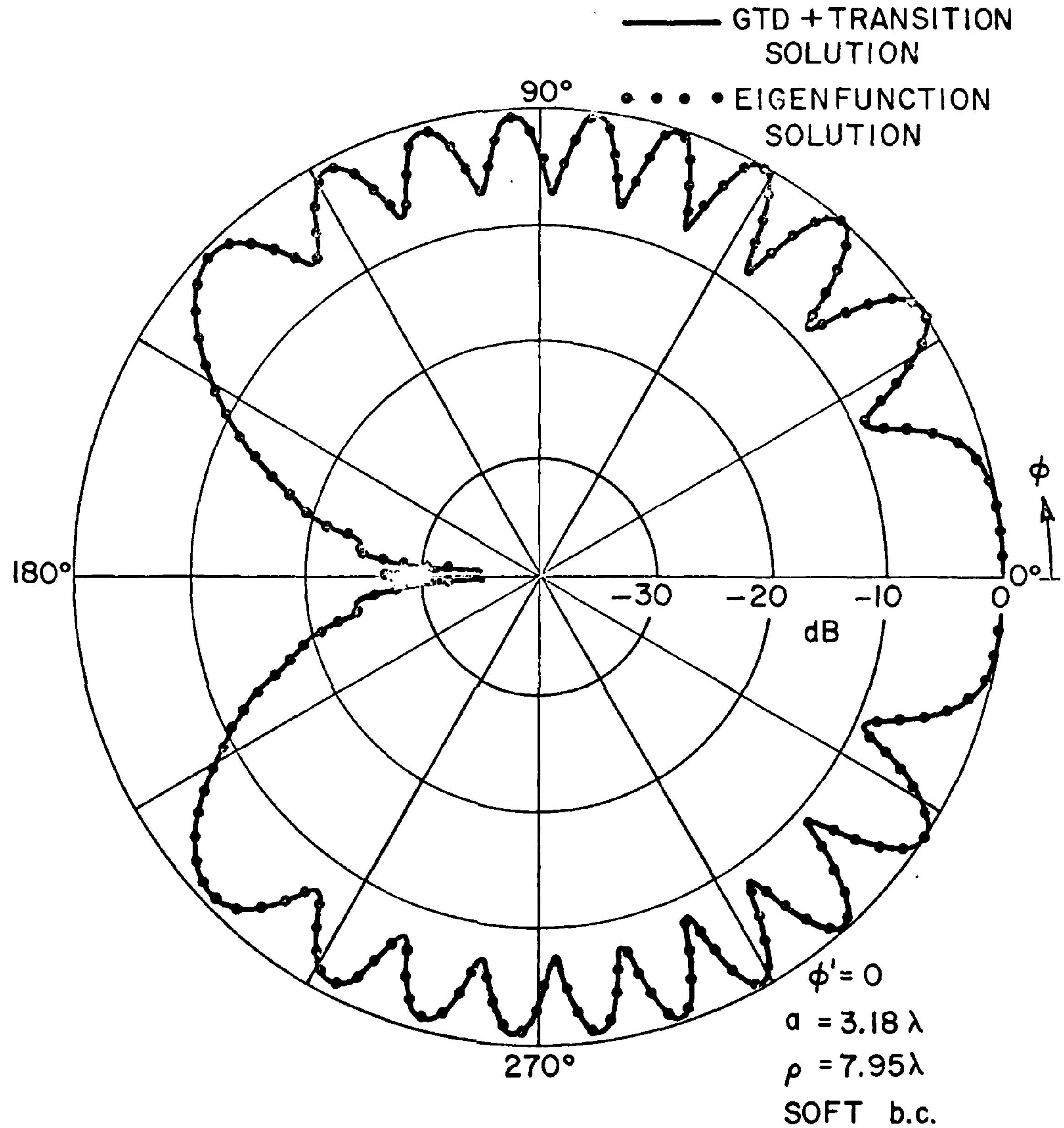

Fig. 22(b). Comparison of the composite GTD plus transition solution of Fig. 22(a) with the exact solution.

IV. SUMMARY AND DISCUSSION

A uniform asymptotic result is developed for describing the fields in the transition regions adjacent to the shadow boundaries which are associated with the problem of plane wave diffraction by a perfectly-conducting, circular cylinder. This result yields a finite, continuous solution for the total field across the shadow boundaries, and exterior to the transition regions it reduces to the usual GTD solution (in terms of the surface diffracted fields and geometrical optical ray fields) for the shadow and lit zones, respectively.

Summarizing this result for convenience, one expresses the total field U exterior to the cylinder via (27) and (49) as

TRANSITION REGION - SHADOW ZONE

$$\text{(51a)}\quad U(P_s) \sim U^i(Q_1)\left[-m\sqrt{\frac{2}{k}}\left(\hat{P}_{\substack{s\\h}}(\xi) + \frac{e^{-i\frac{\pi}{4}}}{2\sqrt{\pi}\xi}\left\{1 - F\left[ks\,\frac{\xi^2}{2m^2}\right]\right\}\right)\right] e^{-ikt}\,\frac{e^{-iks}}{\sqrt{s}}\;;$$

with $\xi = m\theta > 0$,

where $t = a\theta = Q_1Q_2$, $s = Q_2P_s$ as in Fig. 7; and $m = \left(\frac{ka}{2}\right)^{1/3}$. The functions $F[ks\,\frac{\xi^2}{2m^2}]$ and $\hat{P}_{\substack{s\\h}}(\xi)$ are tabulated in Figs. 6 and 8, respectively; one should note that $\hat{P}_s(\xi)$ is associated with the acoustic soft boundary case (TM_z), and $\hat{P}_h(\xi)$ is associated with the acoustic hard boundary case (TE_z). Also, $U^i(Q_1)$ denotes the value of the incident field at Q_1.

TRANSITION REGION - LIT ZONE

$$\text{(51b)}\quad U(P_L) \sim U^i(P_L) + U^i(Q_R)\left[-m\sqrt{\frac{2}{k\rho_r}}\; e^{-i\frac{(\xi')^3}{12}}\right.$$

$$\left.\cdot\left(\hat{P}_{\substack{s\\h}}(\xi') + \frac{e^{-i\frac{\pi}{4}}}{2\sqrt{\pi}\xi'}\left\{1 - F\left[k\ell\,\frac{\xi'^2}{2m^2}\right]\right\}\right)\right]\sqrt{\frac{\rho_r}{\rho_r+\ell}}\; e^{-ik\ell}\;;$$

with $\xi' = -2m\cos\theta^i < 0$,

where $\ell = Q_RP_L$, $\rho_r = \frac{a\cos\theta^i}{2}$; and m, $F[k\ell\,\frac{\xi'^2}{2m^2}]$, $\hat{P}_{\substack{s\\h}}(\xi')$, and U^i have the same meaning as before. The geometrical quantities ℓ, θ^i and the point of reflection Q_R are indicated in Fig. 11. One notes that $\hat{P}_{\substack{s\\h}}(\xi) + \frac{e^{-i\frac{\pi}{4}}}{2\sqrt{\pi}\,\xi} = \begin{Bmatrix} p^*(\xi) \\ q^*(\xi) \end{Bmatrix} e^{-i\frac{\pi}{4}}$ in (51a) and (51b), respectively. The functions p^* and q^* are plotted in Fig. 8.

Equation (51) is valid for both, the near and the far zone; however, in the near zone case, the field point must lie exterior to the surface boundary layer. Within the surface boundary layer, (51a) tends to become singular (as $s \to 0$) in exactly the same manner as the GTD surface diffracted ray field of (33) which becomes singular as $s \to 0$. In order to remove this limitation, one must employ (39) instead of (23) in the analysis as $s \to 0$; however, the case $s \to 0$ is not considered in this paper. One could employ the results of Ivanov [11] which allows the field to be calculated near the surface (within the surface boundary layer) as $s \to 0$. However, as mentioned earlier, his result [11] is in terms of the canonical Fock integral which is complicated for numerical calculations except at $s=0$; when $s=0$, the canonical Fock integral reduces to the single parameter Fock current integral which is well tabulated. It would be worth investigating an alternative approximate solution which matches our solution of (51) outside the surface boundary layer, but which reduces to the Fock currents on the surface ($s=0$), and at the same time is such that it is simple for numerical processing.

The result in (51) yields a finite and continuous field solution across the shadow boundaries. Away from the shadow boundaries, and exterior to the transition region (51a) reduces to the GTD surface diffracted ray field of (33); whereas, (51b) reduces to the geometrical optics incident and reflected ray fields of (37). The $F[\cdot]$ term in (51) dominates in the region at and near the shadow boundaries; whereas, far from the shadow boundaries the $\hat{P}_{\substack{s\\h}}(\cdot)$ term dominates. Since the $F(\cdot)$ and $\hat{P}_{\substack{s\\h}}(\cdot)$ functions are well tabulated [9], the result in (51) is simple to use which makes it well suited to solve practical problems. Furthermore, this result can be readily generalized to convex surfaces of variable curvature in both two and three dimensions by employing the local nature of high frequency fields and reciprocity. These extensions will be presented in a separate paper. Finally, the field at (ρ,ϕ) due to TM_z (or TE_z) plane wave scattering by the cylinder is directly related via reciprocity to the problem of calculating the radiation pattern (along the incident field direction) of an electric (or magnetic) line source at (ρ,ϕ) in the presence of the same cylinder; the latter problem is of interest for estimating the radiation patterns of antennas mounted off the fuselage of a typical aircraft.

REFERENCES

[1] Keller, J. B., "Proceedings of Symposium on Microwave Optics," Part II, McGill University, 1953, pp. 207-210 (AD 211500).

[2] Keller, J. B., "Geometrical Theory of Diffraction," J. Opt. Soc. Am., Vol. 52, No. 2, 1962, pp. 116-130.

[3] Keller, J. B., "Diffraction by a Convex Cylinder," Trans. I.R.E., Vol. AP-24, 1956, pp. 312-321.

[4] Burnside, W. D., "Analysis of On-Aircraft Antenna Patterns," Report 3390-1, August 1972, The Ohio State University Electro-Science Laboratory, Department of Electrical Engineering; prepared under Contract N62269-72-C-0354 for Naval Air Development Center.

[5] Burnside, W. D., Gilreath, M. C., Marhefka, R. J., and Yu, C. L., "A Study of KC-135 Aircraft Antenna Pattern," IEEE Trans. AP-5, May 1975, pp. 309-316.

[6] Fock, V. A., Diffraction, Refraction and Reflection Waves: Thirteen Papers, Air Force Cambridge Research Center Report AFCRC-TN-57-102, June 1957 (AD 117276).

[7] Fock, V. A., "Fresnel Diffraction from Convex Bodies," Uspekii Fizicheskikh Nauk., Vol. 43, 1951, pp. 587-599. (Also in Ref. [6].)

[8] Wait, J. R., and Conda, A. M., "Diffraction of Electromagnetic Waves by Smooth Obstacles," Jour. of Res., N.B.S., Vol. 63D, No. 2, Sept.-Oct., 1959, pp. 181-197.

[9] Logan, N. A., "General Research in Diffraction Theory," Vol. I, LMSD-288087; and Vol. II, LMSD-288088, Missiles and Space Division, Lockheed Aircraft Corp., Dec. 1959.

[10] Logan, N. A., and Yee, K. S., Electromagnetic Waves, Edited by R. E. Langer, Univ. of Wisconsin Press, 1962.

[11] Ivanov, V. I., U.S.S.R. Journal of Computational Math. and Math. Phys. (Translated from Zl. Vychisl. Mat. Mat. Fiz.), Vol. 2, 1971, p. 216.

[12] Borovikov, V. A., and Kinber, B. Y., Proc. IEEE, Vol. 62, No. 11, Nov. 1974, pp. 1416-1437.

[13a] Fock, V. A., "The Field of a Plane Wave Near the Surface of a Conducting Body," Izvestia Akademii Nauk (ser. Fiz.), Vol. 10, 1946, p. 171 (also in [6]).

[13b] Fock, V. A., "The Field of a Vertical and Horizontal Diople Raised Above the Earth's Surface," J. Exp. Theor. Phys. (ZETF), Vol. 19, 1949, p. 916 (also in [6]).

[14] Goriainov, A. S., Radio Eng. Electron (USSR), Vol. 3, 1958, p. 23 (transl. from Radiotechn. i Elektron, Vol. 3, p. 603, 1958).

[15] Felsen, L. B., and Marcuvitz, N., Radiation and Scattering of Waves, Prentice Hall, Inc., Englewood Cliffs, N.J., 1973.

[16] Clemmow, P. C., The Plane Wave Spectrum Representation of Electromagnetic Fields, Pergamon Press, Vol. 12 of Intl. Series of Monographs in Electromagnetic Waves, 1966.

[17] Pathak, P. H., and Kouyoumjian, R. G., "The Dyadic Diffraction Coefficient for a Perfectly-Conducing Wedge," Report 2183-4, June 1970, The Ohio State University ElectroScience Laboratory, Department of Electrical Engineering; prepared under Contract AF 19(628)-5929 for Air Force Cambridge Research Laboratory.

[18] Kouyoumjian, R. G., and Pathak, P. H., Proc. IEEE, Vol. 62, No. 11, Nov. 1974, pp. 1448-1461.

APPENDIX

The result for the geometrical optics field reflected from a perfectly-conducting cylinder which is illuminated with a plane wave is developed in this Appendix; this development is useful to the analysis of section II B. Although this development is available in many texts (e.g., [15]), it is rederived here in terms of the notation employed in section II so that the connection between the results derived here with the analysis in section II B may be established in a convenient fashion. Only the TM_z case is treated here; the results for the TE_z case are exactly the same except for a change of sign.

Referring to Fig. 2, it is seen that the total field exterior to the cylinder in this case is (see (6b)):

$$\text{(A1)} \qquad U \approx \frac{1}{2} \int_{-\infty-i\varepsilon}^{\infty-i\varepsilon} dv \left[H_v^{(1)}(k\rho) - \frac{Q\, H_v^{(1)}(ka)}{Q\, H_v^{(2)}(ka)} H_v^{(2)}(k\rho) \right] e^{-iv[|\phi| - \frac{\pi}{2}]} .$$

For the TM_z case, $Q = 1$, and the first term on the RHS of (A1) yields the incident field [15]; on the other hand, the second term on the RHS of (A1) yields the reflected field for $v<ka$. One is concerned only with this second term which is denoted below by U_r

$$\text{(A2)} \qquad U_r \equiv -\frac{1}{2} \int_{-\infty-i\varepsilon}^{\infty-i\varepsilon} \frac{H_v^{(1)}(ka)}{H_v^{(2)}(ka)} H_v^{(2)}(k\rho)\; e^{-iv[|\phi| - \frac{\pi}{2}]} dv .$$

Employing the Debye approximations in the Hankel functions leads to:

$$\text{(A3)} \qquad U_r \approx -\frac{1}{2} \int_{C_v} e^{-i\frac{\pi}{4}} e^{ik[2\,a \sin \tilde{\gamma} - (\frac{2v}{k} \tilde{\gamma}) - \rho \sin \gamma + \frac{v}{k}\gamma - \frac{v}{k}\psi]} \cdot \sqrt{\frac{2}{\pi k\rho \sin \gamma}}\, dv \quad ,$$

where

$$\text{(A4)} \qquad v = ka \cos \tilde{\gamma} = k\rho \cos \gamma ,$$

and the contour of integration, C_v, is indicated below in Fig. A-I. Also, $\psi = (|\phi| - \pi/2)$ as before.

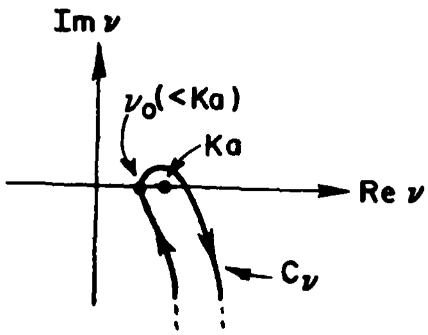

Fig. A-I. Contour of integration C_v.

Rewriting the integral in (A3) as

$$U_r \approx -\sqrt{\frac{1}{2\pi k}}\; e^{-i\frac{\pi}{4}} \int_{C_v} \frac{e^{ikf(v)}}{\sqrt{\rho \sin\gamma}}\, dv \tag{A5}$$

where

$$f(v) \equiv 2\,a \sin\tilde{\gamma} - \left(\frac{2v}{k}\,\tilde{\gamma}\right) - \rho\sin\gamma + \frac{v}{k}\gamma - \frac{v}{k}\psi \quad , \tag{A6}$$

one obtains the following saddle point ($v = v_0$) condition:

$$\left.\frac{\partial f}{\partial v}\right|_{v=v_0} = 0 \quad ; \quad \psi = \gamma_0 - 2\,\tilde{\gamma}_0, \left(\begin{matrix} \gamma = \gamma_0 \text{ at } v = v_0 \\ \tilde{\gamma} = \tilde{\gamma}_0 \text{ at } v = v_0 \end{matrix}\right) . \tag{A7}$$

The following relations hold as a consequence:

(A8) $\cos\theta^i = \sin\tilde{\gamma}_0 \quad , \text{ when } \quad v = v_0 \quad ,$

(A9) $\rho \sin\gamma \Big|_{v=v_0} \cdot \quad = \rho \sin\gamma_0 = \ell + a\sin\tilde{\gamma}_0 = \ell + a\cos\theta^i \quad .$

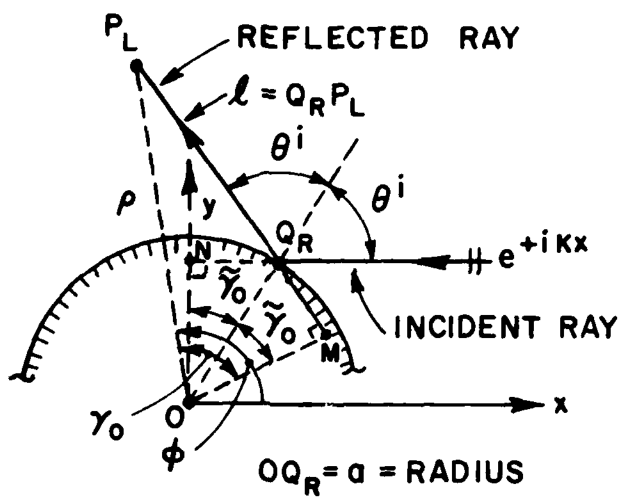

Fig. A-II. Reflected ray geometry.

The geometrical significance of (A7), (A8), and (A9) is shown in Fig. A-II. Also,

$$f(v_0) = a\cos\theta^i - \ell$$
$$f'(v_0) = 0$$
$$f''(v_0) = \frac{2\ \ell + a\cos\theta^i}{(ka\cos\theta^i)(k\rho\sin\gamma_0)} \quad ,$$

where the primes denote differentiation w.r.t. v .

Incorporating the above expressions into the saddle point result for (A5) gives

$$\text{(A10)} \qquad U_r \sim -\sqrt{\frac{1}{2\pi}}\; e^{-i\frac{\pi}{4}} \sqrt{\frac{-2\pi}{ikf''(v_o)}}\; \frac{e^{ikf(v_o)}}{\sqrt{k\rho \sin \gamma_o}} \;.$$

One finally obtains

$$\text{(A11)} \qquad U_r \sim -\, e^{ika \cos \theta^i} \cdot \sqrt{\frac{\frac{a \cos \theta^i}{2}}{\frac{a \cos \theta^i}{2} + \ell}}\; e^{-ik\ell}, \text{ for } TM_z \text{ case;}$$

which in the notation of section II B reduces to

$$\text{(A12)} \qquad U_r \sim R_{\substack{s\\h}} \cdot U^i(Q_R) \sqrt{\frac{\rho_r}{\rho_r + \ell}}\; e^{-ik\ell} \;;\; R_{\substack{s\\h}} = \begin{cases} & TM_z \\ \mp 1; & \\ & TE_z \end{cases} \;,$$

which is the required reflected geometrical optics field.